4.1 Frequency conversion in crystals

G.G. Gurzadyan

4.1.1 Introduction

4.1.1.1 Symbols and abbreviations

4.1.1.1.1 Symbols

η	conversion efficiency
η (energy)	energy conversion efficiency
η (power)	power conversion efficiency
η (quantum)	quantum conversion efficiency
τ_p, τ	pulse duration
α	angle between interacting beams
$\Delta\lambda$	wavelength bandwidth
$\Delta\nu$	frequency bandwidth
$\Delta\theta$	angular bandwidth
E	energy
f	laser pulse repetition rate
I_0	pump intensity
I_thr	threshold intensity
φ_pm	phase-matching angle in the XY plane from X axis
L	crystal length
λ	wavelength
n	refractive index
n_o	ordinary refractive index
n_e	extraordinary refractive index
ν	wave number, frequency
P	power
θ_pm	phase-matching angle from Z axis
ρ	birefringence (walk-off) angle
T, T_pm	crystal temperature

Type I	$\mathrm{o}+\mathrm{o}\rightarrow\mathrm{e}$ or $\mathrm{e}+\mathrm{e}\rightarrow\mathrm{o}$
Type II	$\mathrm{o}+\mathrm{e}\rightarrow\mathrm{e}$ or $\mathrm{o}+\mathrm{e}\rightarrow\mathrm{o}$
ooe	$\mathrm{o}+\mathrm{o}\rightarrow\mathrm{e}$ or $\mathrm{e}\rightarrow\mathrm{o}+\mathrm{o}$
eeo	$\mathrm{e}+\mathrm{e}\rightarrow\mathrm{o}$ or $\mathrm{o}\rightarrow\mathrm{e}+\mathrm{e}$
eoe	$\mathrm{e}+\mathrm{o}\rightarrow\mathrm{e}$ or $\mathrm{e}\rightarrow\mathrm{e}+\mathrm{o}$
oeo	$\mathrm{o}+\mathrm{e}\rightarrow\mathrm{o}$ or $\mathrm{o}\rightarrow\mathrm{e}+\mathrm{o}$

4.1.1.1.2 Abbreviations

av	average
cw	continuous wave
DFG	difference frequency generation
DROPO	doubly resonant OPO
ERR	external ring resonator
FIHG	fifth harmonic generation
FOHG	fourth harmonic generation
ICDFG	intracavity difference frequency generation
ICSHG	intracavity second harmonic generation
IR	infrared
mid IR	middle infrared
NC	noncollinear
NCSHG	noncollinear second harmonic generation
OPA	optical parametric amplifier
OPO	optical parametric oscillator
SFG	sum frequency generation
SH	second harmonic
SHG	second harmonic generation
SIHG	sixth harmonic generation
SP OPO	synchronously pumped OPO
SROPO	singly resonant OPO
SRS	stimulated Raman scattering
THG	third harmonic generation
TROPO	triply resonant OPO
TWOPO	traveling-wave OPO
UV	ultraviolet

4.1.1.1.3 Crystals

Chemical formula	**Symbol**	**Crystal name**
Ag_3AsS_3		Proustite
$AgGaS_2$		Silver Thiogallate
$AgGaSe_2$		Silver Gallium Selenide
Ag_3SbS_3		Pyrargyrite
$Ba_2NaNb_5O_{15}$		Barium Sodium Niobate (Banana)
$\beta-BaB_2O_4$	BBO	Beta-Barium Borate
$CdGeAs_2$		Cadmium Germanium Arsenide
CdSe		Cadmium Selenide
CsB_3O_5	CBO	Cesium Borate
CsH_2AsO_4	CDA	Cesium Dihydrogen Arsenate
$CsLiB_6O_{10}$	CLBO	Cesium Lithium Borate
$C_6H_6N_2O_3$	POM	3-Methyl-4-Nitro-Pyridine-1-Oxide
$C_8H_8O_3$	MHBA	4-Hydroxy-3-Methoxy-Benzaldehyde (Vanillin)
$C_{10}H_{11}N_3O_6$	MAP	Methyl N-(2,4-Dinitrophenyl)-L-Alaninate
$C_{10}H_{13}N_3O_3$	DAN	N-[2-(Dimethylamino)-5-Nitrophenyl]-Acetamide
$C_{11}H_{14}N_2O_3$	NPP	N-(4-Nitrophenyl)-(L)-Propinol
CsD_2AsO_4	DCDA	Cesium Dideuterium Arsenate
GaSe		Gallium Selenide

$HgGa_2S_4$		Mercury Thiogallate
$\alpha-HIO_3$		$\alpha-$Iodic Acid
$KB_5O_8\ 4D_2O$	DKB5	Potassium Pentaborate Tetradeuterate
$KB_5O_8\ 4H_2O$	KB5	Potassium Pentaborate Tetrahydrate
KD_2AsO_4	DKDA	Potassium Dideuterium Arsenate
KD_2PO_4	DKDP	Potassium Dideuterium Phosphate
KH_2PO_4	KDP	Potassium Dihydrogen Phosphate
$KNbO_3$		Potassium Niobate
$KTiOAsO_4$	KTA	Potassium Titanyl Arsenate
$KTiOPO_4$	KTP	Potassium Titanyl Phosphate
LiB_3O_5	LBO	Lithium Triborate
$LiCOOH\ H_2O$	LFM	Lithium Fomate
$LiIO_3$		Lithium Iodate
$LiNbO_3$		Lithium Niobate
$LiNbO_3$:MgO		Mg:O-doped Lithium Niobate
$(NH_2)_2CO$		Urea
$NH_4H_2AsO_4$	ADA	Ammonium Dihydrogen Arsenate
$NH_4H_2PO_4$	ADP	Ammonium Dihydrogen Phosphate
$NO_2C_6H_4NH_2$	mNA	meta-Nitroaniline
RbH_2AsO_4	RDA	Rubidium Dihydrogen Arsenate
RbH_2PO_4	RDP	Rubidium Dihydrogen Phosphate
$RbTiOAsO_4$	RTA	Rubidium Titanyl Arsenate
Te		Tellurium
Tl_3AsSe_3		Thallium Arsenic Selenide
$ZnGeP_2$		Zinc Germanium Phosphide

4.1.1.2 Historical layout

The pioneering work of *Franken et al.* [61Fra] on second harmonic generation of ruby laser radiation in quartz and invention of the phase-matching concept [62Gio, 62Mak] generated a new direction in the freshly born field of nonlinear optics: frequency conversion in crystals. Sum frequency generation by mixing the outputs of two ruby lasers in quartz was already realized in 1962 [62Mil, 62Bas]. *Zernike and Berman* [65Zer] were the first to demonstrate difference frequency mixing. Optical parametric oscillation was experimentally realized in 1965 by *Giordmaine and Miller* [65Gio]. First monographs on nonlinear optics by *Akhmanov and Khokhlov* [64Akh] and *Bloembergen* [65Blo] greatly stimulated development of the nonlinear frequency converters. At present the conversion of laser radiation in nonlinear crystals is a powerful method for generating widely tunable radiation in the ultraviolet, visible, near, mid, and far IR regions.

For theoretical and experimental details of nonlinear frequency conversions in crystals, see monographs by *Zernike and Midwinter* [73Zer], *Danelyus, Piskarskas et al.* [83Dan], *Dmitriev and Tarasov* [87Dmi], *Shen* [84She], Handbook of nonlinear optical crystals (by *Dmitriev, Gurzadyan, Nikogosyan*) [91Dmi, 99Dmi], Handbook of nonlinear optics (by *Sutherland*) [96Sut]. For frequency conversion of femtosecond laser pulses, see also [88Akh]. For linear and nonlinear optical properties of the crystals, see [77Nik, 79Kur, 84Jer, 87Nik, 87Che, 96Sut, 99Dmi, 00Cha, 00Sas]. For related nonlinear phenomena, see [96Sut]. For the historical perspective of the nonlinear frequency conversion over the first forty years, see [00Bye]. In the following section, Sect. 4.1.2, we present some basic equations which may be useful for simple calculations of frequency converters.

4.1.2 Fundamentals

4.1.2.1 Three-wave interactions

Dielectric polarization $\boldsymbol{P}$ (dipole moment of unit volume of the substance) is related to the field $\boldsymbol{E}$ by the material equation of the medium [64Akh, 65Blo] (Chap. 1.1):

$$\boldsymbol{P}(\boldsymbol{E}) = \varepsilon_0 \left(\chi^{(1)}\,\boldsymbol{E} + \chi^{(2)}\,\boldsymbol{E}^2 + \chi^{(3)}\,\boldsymbol{E}^3 + \dots\right) \tag{4.1.1}$$

with

$\varepsilon_0 = 8.854 \times 10^{-12}\ \mathrm{CV^{-1}m^{-1}}$: dielectric permittivity of free space,
$\chi^{(1)} = n^2 - 1$: the linear, and $\chi^{(2)}$, $\chi^{(3)}$ etc.: the nonlinear dielectric susceptibilities.

In the present chapter, Chap. 4.1, we consider only three-wave interactions in crystals with square nonlinearity ($\chi^{(2)} \neq 0$). The following nonlinear frequency conversion processes are considered:

Second Harmonic Generation (SHG):

$$\omega + \omega = 2\,\omega\ , \tag{4.1.2}$$

Sum-Frequency Generation (SFG) or up-conversion:

$$\omega_1 + \omega_2 = \omega_3\ , \tag{4.1.3}$$

Difference-Frequency Generation (DFG) or down-conversion:

$$\omega_3 - \omega_2 = \omega_1\ , \tag{4.1.4}$$

Optical Parametric Oscillation (OPO):

$$\omega_3 = \omega_2 + \omega_1\ . \tag{4.1.5}$$

For efficient frequency conversion *phase matching* should be fulfilled:

$$\boldsymbol{k}_1 + \boldsymbol{k}_2 = \boldsymbol{k}_3 \tag{4.1.6}$$

with

$\boldsymbol{k}_i$: the wave vectors for ω_1 , ω_2 , ω_3 , respectively.

Two types of phase matching are introduced:

type I: $\mathrm{o} + \mathrm{o} \rightarrow \mathrm{e}$ or $\mathrm{e} + \mathrm{e} \rightarrow \mathrm{o}$,
type II: $\mathrm{o} + \mathrm{e} \rightarrow \mathrm{e}$ or $\mathrm{o} + \mathrm{e} \rightarrow \mathrm{o}$,

or with shortened notations:

ooe: $\mathrm{o} + \mathrm{o} \rightarrow \mathrm{e}$ or $\mathrm{e} \rightarrow \mathrm{o} + \mathrm{o}$,
eeo: $\mathrm{e} + \mathrm{e} \rightarrow \mathrm{o}$ or $\mathrm{o} \rightarrow \mathrm{e} + \mathrm{e}$,
eoe: $\mathrm{e} + \mathrm{o} \rightarrow \mathrm{e}$ or $\mathrm{e} \rightarrow \mathrm{e} + \mathrm{o}$,
oeo: $\mathrm{o} + \mathrm{e} \rightarrow \mathrm{o}$ or $\mathrm{o} \rightarrow \mathrm{e} + \mathrm{o}$.

In the shortened notation (ooe, eoe, ...) applies: $\omega_1 < \omega_2 < \omega_3$, i.e. the first symbol refers to the longest-wavelength radiation, and the latter to the shortest-wavelength radiation. Here, *o-beam*, or ordinary beam, is the beam with polarization normal to the principal plane of the crystal, i.e.

the plane containing the wave vector $\boldsymbol{k}$ and crystallophysical axis Z (or optical axis, for uniaxial crystals). The *e-beam*, or extraordinary beam, is the beam with polarization in the principal plane.

The methods of angular and temperature phase-matching tuning are used in frequency converters. Angular tuning is rather simple and more rapid than temperature tuning. Temperature tuning is generally used in the case of 90 ° phase matching, i.e., when the birefringence angle is zero. This method is mainly used in crystals with a strong temperature dependence of phase matching: $LiNbO_3$, LBO, $KNbO_3$, and $Ba_2NaNb_5O_{15}$.

4.1.2.2 Uniaxial crystals

For uniaxial crystals the difference between the refractive indices of the ordinary and extraordinary beams, *birefringence* Δn, is zero along the optical axis (crystallophysical axis Z) and maximum in the normal direction. The refractive index of the ordinary beam does not depend on the direction of propagation, however, the refractive index of the extraordinary beam $n_e(\theta)$ is a function of the polar angle θ between the Z axis and the vector $\boldsymbol{k}$ (but not of the azimuthal angle φ) (Fig. 4.1.1):

$$n_e(\theta) = n_o \left[\frac{1 + \tan^2\theta}{1 + \left(\frac{n_o}{n_e}\right)^2 \tan^2\theta} \right]^{\frac{1}{2}}, \tag{4.1.7}$$

where n_o and n_e are the refractive indices of the ordinary and extraordinary beams in the plane normal to the Z axis and termed as corresponding *principal values*. Note that if $n_o > n_e$, the crystal is *negative*, and if $n_o < n_e$, it is *positive*. For an o-beam the indicatrix of the refractive indices is a sphere with radius n_o, and an ellipsoid of rotation with semiaxes n_o and n_e for an e-beam (Fig. 4.1.2). In the crystal the beam, in general, is divided into two beams with orthogonal polarizations; the angle between these beams ρ is the *birefringence* (or *walk-off*) angle.

Equations for calculating phase-matching angles in uniaxial crystals are given in Table 4.1.1 [86Nik, 99Dmi].

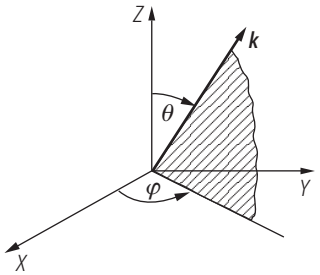

Fig. 4.1.1. Polar coordinate system for description of refraction properties of uniaxial crystals ($\boldsymbol{k}$ is the light propagation direction, Z is the optic axis, θ and φ are the coordinate angles).

4.1.2.3 Biaxial crystals

For biaxial crystals the optical indicatrix has a bilayer surface with four points of interlayer contact which correspond to the directions of two optical axis. In the simple case of light propagation in

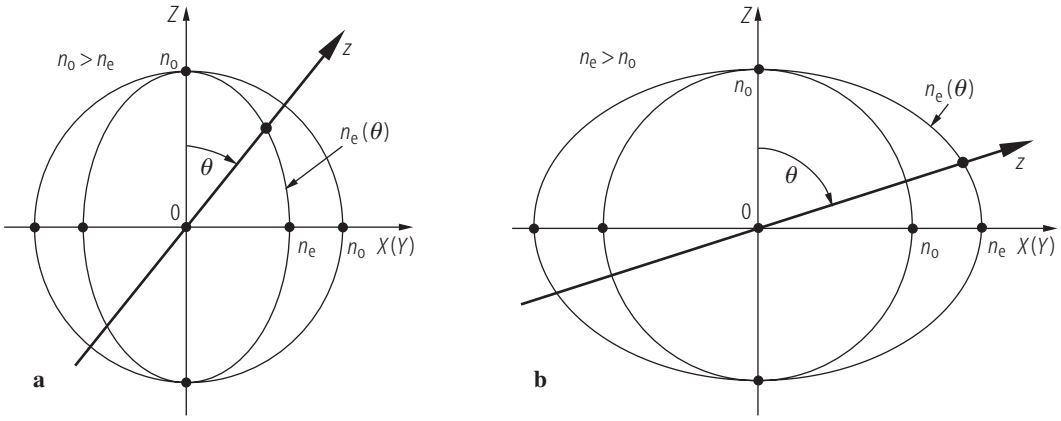

Fig. 4.1.2. Dependence of refractive index on light propagation direction and polarization (index surface) in uniaxial crystals: **(a)** negative: $n_o > n_e$ and **(b)** positive: $n_e > n_o$.

Table 4.1.1. Equations for calculating phase-matching angles in uniaxial crystals [86Nik, 99Dmi].

Negative uniaxial crystals	Positive uniaxial crystals
$\tan^2\theta_{pm}^{ooe} = (1-U)/(W-1)$	$\tan^2\theta_{pm}^{eeo} \approx (1-U)/(U-S)$
$\tan^2\theta_{pm}^{eoe} \approx (1-U)/(W-R)$	$\tan^2\theta_{pm}^{oeo} = (1-V)/(V-Y)$
$\tan^2\theta_{pm}^{oee} \approx (1-U)/(W-Q)$	$\tan^2\theta_{pm}^{eoo} = (1-T)/(T-Z)$

Notations:

$U = (A+B)^2/C^2$; $W = (A+B)^2/F^2$; $R = (A+B)^2/(D+B)^2$;
$Q = (A+B)^2/(A+E)^2$; $S = (A+B)^2/(D+E)^2$; $V = B^2/(C-A)^2$;
$Y = B^2/E^2$; $T = A^2/(C-B)^2$; $Z = A^2/D^2$;
$A = n_{o1}/\lambda_1$; $B = n_{o2}/\lambda_2$; $C = n_{o3}/\lambda_3$;
$D = n_{e1}/\lambda_1$; $E = n_{e2}/\lambda_2$; $F = n_{e3}/\lambda_3$.

These expressions can be generalized to noncollinear phase matching. In this case, for example, the phase-matching angle θ_{pm}^{ooe} is determined from the above presented equation using the new coefficients U and W:

$$U = (A^2 + B^2 + 2AB\cos\gamma)/C^2\,,\ W = (A^2 + B^2 + 2AB\cos\gamma)/F^2\,,$$

where γ is the angle between the wave vectors $\boldsymbol{k}_1$ and $\boldsymbol{k}_2$.

the principal planes XY, YZ, and XZ the dependencies of refractive indices on the direction of light propagation represent a combination of an ellipse and a circle (Fig. 4.1.3). Thus in the principal planes a biaxial crystal can be considered as a uniaxial crystal, e.g. a biaxial crystal with $n_Z > n_Y > n_X$ in the XY plane is similar to a negative uniaxial crystal with $n_o = n_Z$ and

$$n_e(\varphi) = n_Y \left(\frac{1 + \tan^2\varphi}{1 + (n_Y/n_X)^2 \tan^2\varphi} \right)^{\frac{1}{2}} . \tag{4.1.8}$$

The angle V_Z between the optical axis and Z axis for the case $n_Z > n_Y > n_X$ can be found from:

$$\sin V_Z = \frac{n_Z}{n_Y} \left(\frac{n_Y^2 - n_X^2}{n_Z^2 - n_X^2} \right)^{\frac{1}{2}} \tag{4.1.9}$$

and for the case $n_X > n_Y > n_Z$:

$$\cos V_Z = \frac{n_X}{n_Y} \left(\frac{n_Y^2 - n_Z^2}{n_X^2 - n_Z^2} \right)^{\frac{1}{2}} . \tag{4.1.10}$$

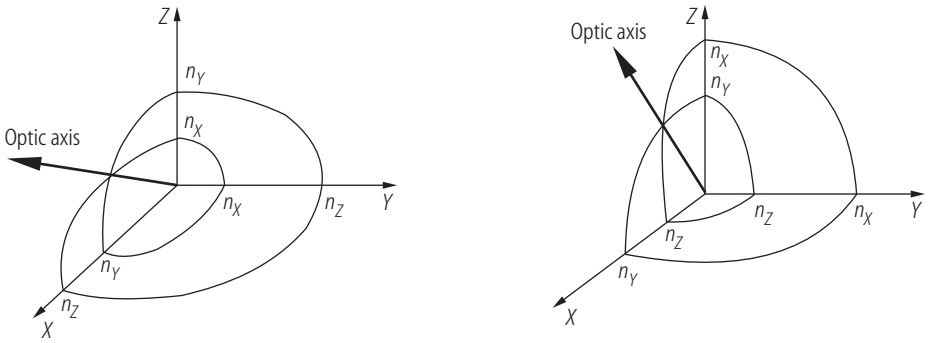

Fig. 4.1.3. Dependence of refractive index on light propagation direction and polarization (index surface) in biaxial crystals: **(a)** $n_X < n_Y < n_Z$, **(b)** $n_X > n_Y > n_Z$.

For a positive biaxial crystal the bisectrix of the acute angle between optical axes coincides with $n_{\max}$ and for a negative one the bisectrix coincides with $n_{\min}$.

Equations for calculating phase-matching angles upon propagation in principal planes of biaxial crystals are given in Table 4.1.2 [87Nik, 99Dmi].

4.1.2.4 Effective nonlinearity

Miller delta formulation [64Mil]:

$$\varepsilon_0 E_i(\omega_3) = \delta_{ijk} P_j(\omega_1) P_k(\omega_2) \,, \tag{4.1.11}$$

where the Miller coefficient,

$$\delta_{ijk} = \frac{1}{2\varepsilon_0} \, \frac{\chi^{(2)}_{ijk}(\omega_3)}{\chi^{(1)}_{ii}(\omega_1)\, \chi^{(1)}_{jj}(\omega_2)\, \chi^{(1)}_{kk}(\omega_3)} \,, \tag{4.1.12}$$

has small dispersion and is almost constant for a wide range of crystals.

For anisotropic media the coefficients $\chi^{(1)}$ and $\chi^{(2)}$ are, in general, the second- and third-rank tensors, respectively. In practice, the tensor

$$d_{ijk} = \frac{1}{2}\, \chi_{ijk} \tag{4.1.13}$$

is used instead of χ_{ijk} . Usually, the "plane" representation of d_{ijk} in the form d_{il} is used, the relation between l and jk is:

jk		l
11	$\leftrightarrow$	1
22	$\leftrightarrow$	2
33	$\leftrightarrow$	3
23 or 32	$\leftrightarrow$	4
31 or 13	$\leftrightarrow$	5
12 or 21	$\leftrightarrow$	6

Table 4.1.2. Equations for calculating phase-matching angles in biaxial crystals upon light propagation in the principal planes [87Nik, 99Dmi].

(a) $n_X < n_Y < n_Z$

Principal plane	Type of interaction	Equations	Notations
	ooe	$\tan^2\varphi = \dfrac{1-U}{W-1}$	$U = \left(\dfrac{A+B}{C}\right)^2$; $W = \left(\dfrac{A+B}{F}\right)^2$; $A = \dfrac{n_{Z1}}{\lambda_1}$; $B = \dfrac{n_{Z2}}{\lambda_2}$; $C = \dfrac{n_{Y3}}{\lambda_3}$; $F = \dfrac{n_{X3}}{\lambda_3}$
XY	eoe	$\tan^2\varphi \approx \dfrac{1-U}{W-R}$	$U = \left(\dfrac{A+B}{C}\right)^2$; $W = \left(\dfrac{A+B}{F}\right)^2$; $R = \left(\dfrac{A+B}{D+B}\right)^2$; $A = \dfrac{n_{Y1}}{\lambda_1}$; $B = \dfrac{n_{Z2}}{\lambda_2}$; $C = \dfrac{n_{Y3}}{\lambda_3}$; $D = \dfrac{n_{X1}}{\lambda_1}$; $F = \dfrac{n_{X3}}{\lambda_3}$
	oee	$\tan^2\varphi \approx \dfrac{1-U}{W-Q}$	$U = \left(\dfrac{A+B}{C}\right)^2$; $W = \left(\dfrac{A+B}{F}\right)^2$; $Q = \left(\dfrac{A+B}{A+E}\right)^2$; $A = \dfrac{n_{Z1}}{\lambda_1}$; $B = \dfrac{n_{Y2}}{\lambda_2}$; $C = \dfrac{n_{Y3}}{\lambda_3}$; $E = \dfrac{n_{X2}}{\lambda_2}$; $F = \dfrac{n_{X3}}{\lambda_3}$
	eeo	$\tan^2\theta \approx \dfrac{1-U}{U-S}$	$U = \left(\dfrac{A+B}{C}\right)^2$; $S = \left(\dfrac{A+B}{D+E}\right)^2$; $A = \dfrac{n_{Y1}}{\lambda_1}$; $B = \dfrac{n_{Y2}}{\lambda_2}$; $C = \dfrac{n_{X3}}{\lambda_3}$; $D = \dfrac{n_{Z1}}{\lambda_1}$; $E = \dfrac{n_{Z2}}{\lambda_2}$
YZ	oeo	$\tan^2\theta = \dfrac{1-V}{V-Y}$	$V = \left(\dfrac{B}{C-A}\right)^2$; $Y = \left(\dfrac{B}{E}\right)^2$; $A = \dfrac{n_{X1}}{\lambda_1}$; $B = \dfrac{n_{Y2}}{\lambda_2}$; $C = \dfrac{n_{X3}}{\lambda_3}$; $E = \dfrac{n_{Z2}}{\lambda_2}$
	eoo	$\tan^2\theta = \dfrac{1-T}{T-Z}$	$T = \left(\dfrac{A}{C-B}\right)^2$; $Z = \left(\dfrac{A}{D}\right)^2$; $A = \dfrac{n_{Y1}}{\lambda_1}$; $B = \dfrac{n_{X2}}{\lambda_2}$; $C = \dfrac{n_{X3}}{\lambda_3}$; $D = \dfrac{n_{Z1}}{\lambda_1}$
XZ	ooe	$\tan^2\theta = \dfrac{1-U}{W-1}$	$U = \left(\dfrac{A+B}{C}\right)^2$; $W = \left(\dfrac{A+B}{F}\right)^2$; $A = \dfrac{n_{Y1}}{\lambda_1}$; $B = \dfrac{n_{Y2}}{\lambda_2}$; $C = \dfrac{n_{X3}}{\lambda_3}$; $F = \dfrac{n_{Z3}}{\lambda_3}$
$\theta < V_Z$	eoe	$\tan^2\theta \approx \dfrac{1-U}{W-R}$	$U = \left(\dfrac{A+B}{C}\right)^2$; $W = \left(\dfrac{A+B}{F}\right)^2$; $R = \left(\dfrac{A+B}{D+B}\right)^2$; $A = \dfrac{n_{X1}}{\lambda_1}$; $B = \dfrac{n_{Y2}}{\lambda_2}$; $C = \dfrac{n_{X3}}{\lambda_3}$; $D = \dfrac{n_{Z1}}{\lambda_1}$; $F = \dfrac{n_{Z3}}{\lambda_3}$
	oee	$\tan^2\theta \approx \dfrac{1-U}{W-Q}$	$U = \left(\dfrac{A+B}{C}\right)^2$; $W = \left(\dfrac{A+B}{F}\right)^2$; $Q = \left(\dfrac{A+B}{A+E}\right)^2$; $A = \dfrac{n_{Y1}}{\lambda_1}$; $B = \dfrac{n_{X2}}{\lambda_2}$; $C = \dfrac{n_{X3}}{\lambda_3}$; $E = \dfrac{n_{Z2}}{\lambda_2}$; $F = \dfrac{n_{Z3}}{\lambda_3}$
XZ	eeo	$\tan^2\theta \approx \dfrac{1-U}{U-S}$	$U = \left(\dfrac{A+B}{C}\right)^2$; $S = \left(\dfrac{A+B}{D+E}\right)^2$; $A = \dfrac{n_{X1}}{\lambda_1}$; $B = \dfrac{n_{X2}}{\lambda_2}$; $C = \dfrac{n_{Y3}}{\lambda_3}$; $D = \dfrac{n_{Z1}}{\lambda_3}$; $E = \dfrac{n_{Z2}}{\lambda_2}$
$\theta > V_Z$	oeo	$\tan^2\theta = \dfrac{1-V}{V-Y}$	$V = \left(\dfrac{B}{C-A}\right)^2$; $Y = \left(\dfrac{B}{E}\right)^2$; $A = \dfrac{n_{Y1}}{\lambda_1}$; $B = \dfrac{n_{X2}}{\lambda_2}$; $C = \dfrac{n_{Y3}}{\lambda_3}$; $E = \dfrac{n_{Z2}}{\lambda_2}$
	eoo	$\tan^2\theta = \dfrac{1-T}{T-Z}$	$T = \left(\dfrac{A}{C-B}\right)^2$; $Z = \left(\dfrac{A}{D}\right)^2$; $A = \dfrac{n_{X1}}{\lambda_1}$; $B = \dfrac{n_{Y2}}{\lambda_2}$; $C = \dfrac{n_{Y3}}{\lambda_3}$; $D = \dfrac{n_{Z1}}{\lambda_1}$

(continued)

Table 4.1.2 continued.

(b) $n_X > n_Y > n_Z$

Principal plane	Type of interaction	Equations	Notations
	eeo	$\tan^2\varphi \approx \frac{1-U}{U-S}$	$U=\left(\frac{A+B}{C}\right)^2;\ S=\left(\frac{A+B}{D+E}\right)^2;\ A=\frac{n_{Y1}}{\lambda_1};\ B=\frac{n_{Y2}}{\lambda_2};\ C=\frac{n_{Z3}}{\lambda_3};\ D=\frac{n_{X1}}{\lambda_1};\ E=\frac{n_{X2}}{\lambda_2}$
XY	oeo	$\tan^2\varphi = \frac{1-V}{V-Y}$	$V=\left(\frac{B}{C-A}\right)^2;\ Y=\left(\frac{B}{E}\right)^2;\ A=\frac{n_{Z1}}{\lambda_1};\ B=\frac{n_{Y2}}{\lambda_2};\ C=\frac{n_{Z3}}{\lambda_3};\ E=\frac{n_{X2}}{\lambda_2}$
	eoo	$\tan^2\varphi = \frac{1-T}{T-Z}$	$T=\left(\frac{A}{C-B}\right)^2;\ Z=\left(\frac{A}{D}\right)^2;\ A=\frac{n_{Y1}}{\lambda_1};\ B=\frac{n_{Z2}}{\lambda_2};\ C=\frac{n_{Z3}}{\lambda_3};\ D=\frac{n_{X1}}{\lambda_1}$
	ooe	$\tan^2\theta = \frac{1-U}{W-1}$	$U=\left(\frac{A+B}{C}\right)^2;\ W=\left(\frac{A+B}{F}\right)^2;\ A=\frac{n_{X1}}{\lambda_1};\ B=\frac{n_{X2}}{\lambda_2};\ C=\frac{n_{Y3}}{\lambda_3};\ F=\frac{n_{Z3}}{\lambda_3}$
YZ	eoe	$\tan^2\theta \approx \frac{1-U}{W-R}$	$U=\left(\frac{A+B}{C}\right)^2;\ W=\left(\frac{A+B}{F}\right)^2;\ R=\left(\frac{A+B}{D+B}\right)^2;\ A=\frac{n_{Y1}}{\lambda_1};\ B=\frac{n_{X2}}{\lambda_2};\ C=\frac{n_{Y3}}{\lambda_3};\ D=\frac{n_{Z1}}{\lambda_1};\ F=\frac{n_{Z3}}{\lambda_3}$
	oee	$\tan^2\theta \approx \frac{1-U}{W-Q}$	$U=\left(\frac{A+B}{C}\right)^2;\ W=\left(\frac{A+B}{F}\right)^2;\ Q=\left(\frac{A+B}{A+E}\right)^2;\ A=\frac{n_{X1}}{\lambda_1};\ B=\frac{n_{Y2}}{\lambda_2};\ C=\frac{n_{Y3}}{\lambda_3};\ E=\frac{n_{Z2}}{\lambda_2};\ F=\frac{n_{Z3}}{\lambda_3}$
XZ	eeo	$\tan^2\theta \approx \frac{1-U}{U-S}$	$U=\left(\frac{A+B}{C}\right)^2;\ S=\left(\frac{A+B}{D+E}\right)^2;\ A=\frac{n_{X1}}{\lambda_1};\ B=\frac{n_{X2}}{\lambda_2};\ C=\frac{n_{Y3}}{\lambda_3};\ D=\frac{n_{Z1}}{\lambda_1};\ E=\frac{n_{Z2}}{\lambda_2}$
$\theta < V_Z$	oeo	$\tan^2\theta = \frac{1-V}{V-Y}$	$V=\left(\frac{B}{C-A}\right)^2;\ Y=\left(\frac{B}{E}\right)^2;\ A=\frac{n_{Y1}}{\lambda_1};\ B=\frac{n_{X2}}{\lambda_2};\ C=\frac{n_{Y3}}{\lambda_3};\ E=\frac{n_{Z2}}{\lambda_2}$
	eoo	$\tan^2\theta = \frac{1-T}{T-Z}$	$T=\left(\frac{A}{C-B}\right)^2;\ Z=\left(\frac{A}{D}\right)^2;\ A=\frac{n_{X1}}{\lambda_1};\ B=\frac{n_{Y2}}{\lambda_2};\ C=\frac{n_{Y3}}{\lambda_3};\ D=\frac{n_{Z1}}{\lambda_1}$
	ooe	$\tan^2\theta = \frac{1-U}{W-1}$	$U=\left(\frac{A+B}{C}\right)^2;\ W=\left(\frac{A+B}{F}\right)^2;\ A=\frac{n_{Y1}}{\lambda_1};\ B=\frac{n_{Y2}}{\lambda_2};\ C=\frac{n_{X3}}{\lambda_3};\ F=\frac{n_{Z3}}{\lambda_3}$
XZ	eoe	$\tan^2\theta \approx \frac{1-U}{W-R}$	$U=\left(\frac{A+B}{C}\right)^2;\ W=\left(\frac{A+B}{F}\right)^2;\ R=\left(\frac{A+B}{D+B}\right)^2;\ A=\frac{n_{X1}}{\lambda_1};\ B=\frac{n_{Y2}}{\lambda_2};\ C=\frac{n_{X3}}{\lambda_3};\ D=\frac{n_{Z1}}{\lambda_1};\ F=\frac{n_{Z3}}{\lambda_3}$
$\theta > V_Z$	oee	$\tan^2\theta \approx \frac{1-U}{W-Q}$	$U=\left(\frac{A+B}{C}\right)^2;\ W=\left(\frac{A+B}{F}\right)^2;\ Q=\left(\frac{A+B}{A+E}\right)^2;\ A=\frac{n_{Y1}}{\lambda_1};\ B=\frac{n_{X2}}{\lambda_2};\ C=\frac{n_{X3}}{\lambda_3};\ E=\frac{n_{Z2}}{\lambda_2};\ F=\frac{n_{Z3}}{\lambda_3}$

Kleinman symmetry conditions [62Kle]: $d_{21} = d_{16}$, $d_{24} = d_{32}$, $d_{31} = d_{15}$, $d_{13} = d_{35}$, $d_{14} = d_{36}$, $d_{25} = d_{12} = d_{26}$, $d_{32} = d_{24}$ are valid in the case of non-dispersion of electron nonlinear polarizability. The equations for calculating the conversion efficiency include the effective nonlinear coefficients d_{eff}, which comprise all summation operations along the polarization directions of the interacting waves and thus reduce the calculation to one dimension. Effective nonlinearities d_{eff} for different crystal point groups under valid *Kleinman symmetry* conditions are presented in Table 4.1.3.

The conversion factors for SI and CGS-esu systems are given in Table 4.1.4.

Table 4.1.3. Expressions for d_{eff} in nonlinear crystals when *Kleinman symmetry* relations are valid.

(a) Uniaxial crystals

Point group	Type of interaction ooe, oeo, eoo	eeo, eoe, oee
4, $4mm$	$d_{15} \sin\theta$	0
6, $6mm$	$d_{15} \sin\theta$	0
$\bar{6}m2$	$d_{22} \cos\theta \sin(3\varphi)$	$d_{22} \cos^2\theta \cos\varphi$
$3m$	$d_{15} \sin\theta - d_{22} \cos\theta \sin(3\varphi)$	$d_{22} \cos^2\theta \cos(3\varphi)$
$\bar{6}$	$(d_{11} \cos(3\varphi) - d_{22} \sin(3\varphi)) \cos\theta$	$(d_{11} \sin(3\varphi) + d_{22} \cos(3\varphi)) \cos^2\theta$
3	$(d_{11} \cos(3\varphi) - d_{22} \sin(3\varphi)) \cos\theta + d_{15} \sin\theta$	$(d_{11} \sin(3\varphi) + d_{22} \cos(3\varphi)) \cos^2\theta$
32	$d_{11} \cos\theta \cos(3\varphi)$	$d_{11} \cos^2\theta \sin(3\varphi)$
$\bar{4}$	$(d_{14} \sin(2\varphi) + d_{15} \cos(2\varphi)) \sin\theta$	$(d_{14} \cos(2\varphi) - d_{15} \sin(2\varphi)) \sin(2\theta)$
$\bar{4}2m$	$d_{36} \sin\theta \sin(2\varphi)$	$d_{36} \sin(2\theta) \cos(2\varphi)$

(b) Biaxial crystals (assignments of crystallophysical and crystallographic axes: for $mm2$ and 222 point groups: $X, Y, Z \to a, b, c$; for 2 and m point groups: $Y \to b$)

Point group	Principal plane	Type of interaction ooe, oeo, eoo	eeo, eoe, oee
2	XY	$d_{23} \cos\varphi$	$d_{36} \sin(2\varphi)$
	YZ	$d_{21} \cos\theta$	$d_{36} \sin(2\theta)$
	XZ	0	$d_{21} \cos^2\theta + d_{23} \sin^2\theta - d_{36} \sin(2\theta)$
m	XY	$d_{13} \sin\varphi$	$d_{31} \sin^2\varphi + d_{32} \cos^2\varphi$
	YZ	$d_{31} \sin\theta$	$d_{13} \sin^2\theta + d_{12} \cos^2\theta$
	XZ	$d_{12} \cos\theta - d_{32} \sin\theta$	0
$mm2$	XY	0	$d_{31} \sin^2\varphi + d_{32} \cos^2\varphi$
	YZ	$d_{31} \sin\theta$	0
	XZ	$d_{32} \sin\theta$	0
222	XY	0	$d_{36} \sin(2\varphi)$
	YZ	0	$d_{36} \sin(2\theta)$
	XZ	0	$d_{36} \sin(2\theta)$

Table 4.1.4. Units and conversion factors.

Nonlinear coefficient	MKS or SI units		CGS or electrostatic units
$\chi_{ij}^{(1)}$	1 (SI, dimensionless)	=	$\frac{1}{4\pi}$ (esu, dimensionless)
d_{ij} or $\chi_{ijk}^{(2)}$	1 $V^{-1}m$	=	$\frac{3\times10^4}{4\pi}$ $(erg^{-1}\,cm^3)^{\frac{1}{2}}$
δ_{ij}	1 $C^{-1}m^2$	=	$\frac{4\pi}{3\times10^5}$ $(erg^{-1}\,cm^3)^{\frac{1}{2}}$

Note that in SI units $\boldsymbol{P}^{(n)} = \varepsilon_0\,\boldsymbol{\chi}^{(n)}\boldsymbol{E}^n$ (with $\boldsymbol{P}^{(n)}$ expressed in C m^{-2}), whereas in CGS or esu units $\boldsymbol{P}^{(n)} = \boldsymbol{\chi}^{(n)}\boldsymbol{E}^n$ (with $\boldsymbol{P}^{(n)}$ expressed in esu).

4.1.2.5 Frequency conversion efficiency

4.1.2.5.1 General approach

The conversion efficiency of a three-wave interaction process for the case of square nonlinearity

$$\boldsymbol{P}_{\rm nl} = \varepsilon_0\,\chi^{(2)}\boldsymbol{E}^2 \tag{4.1.14}$$

can be determined from the wave equation derived from Maxwell's equations [64Akh, 65Blo, 73Zer, 99Dmi], see also (1.1.4)–(1.1.7),

$$\nabla\times\nabla\times\boldsymbol{E} + \frac{(1+\chi^{(1)})}{c^2}\,\frac{\partial^2\boldsymbol{E}}{\partial t^2} = -\frac{1}{\varepsilon_0\,c^2}\,\frac{\partial^2\boldsymbol{P}_{\rm nl}}{\partial t^2} \tag{4.1.15}$$

with the initial and boundary conditions for the electric field $\boldsymbol{E}$.

An exact calculation of the nonlinear conversion efficiency for SHG, SFG, and DFG generally requires a numerical calculation. In some simple cases analytical expressions are available. In order to choose the proper method, the contribution of different effects in the nonlinear mixing process should be determined. For this purpose the following approach is introduced [99Dmi]:

– Consider the *effective lengths* of the interaction process:

1. Aperture length $L_{\rm a}$:

$$L_{\rm a} = d_0\,\rho^{-1}\,, \tag{4.1.16}$$

where d_0 is the beam diameter.

2. Quasistatic interaction length $L_{\rm qs}$:

$$L_{\rm qs} = \tau\nu^{-1}\,, \tag{4.1.17}$$

where τ is the radiation pulse width and ν is the mismatch of reverse group velocities. For SHG

$$\nu = u_\omega^{-1} - u_{2\omega}^{-1}\,, \tag{4.1.18}$$

where u_ω and $u_{2\omega}$ are the group velocities of the corresponding waves ω and 2ω.

3. Diffraction length $L_{\rm dif}$:

$$L_{\rm dif} = k\,d_0^2\,. \tag{4.1.19}$$

4. Dispersion-spreading length $L_{\rm ds}$:

$$L_{\rm ds} = \tau^2 g^{-1}\,, \tag{4.1.20}$$

where g is the dispersion-spreading coefficient

$$g = \frac{1}{2}\left(\frac{\partial^2 k}{\partial \omega^2}\right) . \tag{4.1.21}$$

5. Nonlinear interaction length L_{nl}:

$$L_{\mathrm{nl}} = (\sigma\, a_0)^{-1} . \tag{4.1.22}$$

Here σ is the nonlinear coupling coefficient:

$$\sigma_{1,2} = 4\,\pi\, k_{1,2}\, n_{1,2}^{-2}\, d_{\mathrm{eff}} , \tag{4.1.23}$$

$$\sigma_3 = 2\,\pi\, k_3\, n_3^{-2}\, d_{\mathrm{eff}} , \tag{4.1.24}$$

and

$$a_0 = \left(a_1^2\,(0) + a_2^2\,(0) + a_3^2\,(0)\right)^{\frac{1}{2}} , \tag{4.1.25}$$

where $a_n(0)$ are the wave amplitudes of interacting waves λ_1, λ_2, and λ_3 at the input surface of the crystal.

– The length of the crystal L should be compared with L_{eff} from above equations. If $L < L_{\mathrm{eff}}$ the respective effect can be neglected.

4.1.2.5.2 Plane-wave fixed-field approximation

When the conditions $L < L_{\mathrm{nl}}$ and $L < L_{\mathrm{eff}}$ are fulfilled, the so-called fixed-field approximation is realized. For SHG, $\omega + \omega = 2\omega$ and $\Delta k = 2k_\omega - k_{2\omega}$, the conversion efficiency η is determined by the equation:

$$\eta = P_{2\omega}/P_\omega = \frac{2\,\pi^2 d_{\mathrm{eff}}^2 L^2 P_\omega}{\varepsilon_0\, c\, n_\omega^2\, n_{2\,\omega}\, \lambda_2^2\, A}\ \mathrm{sinc}^2\left(\frac{|\Delta k|\, L}{2}\right) . \tag{4.1.26}$$

For SFG, $\omega_1 + \omega_2 = \omega_3$ and $\Delta k = k_1 + k_2 - k_3$, the conversion efficiency η is:

$$\eta = P_3/P_1 = \frac{8\,\pi^2 d_{\mathrm{eff}}^2 L^2 P_2}{\varepsilon_0\, c\, n_1\, n_2\, n_3\, \lambda_3^2\, A}\ \mathrm{sinc}^2\left(\frac{|\Delta k|\, L}{2}\right) . \tag{4.1.27}$$

For DFG, $\omega_1 = \omega_3 - \omega_2$ and $\Delta k = k_1 + k_2 - k_3$, the conversion efficiency η is:

$$\eta = P_1/P_3 = \frac{8\,\pi^2 d_{\mathrm{eff}}^2 L^2 P_2}{\varepsilon_0\, c\, n_1\, n_2\, n_3\, \lambda_1^2\, A}\ \mathrm{sinc}^2\left(\frac{|\Delta k|\, L}{2}\right) . \tag{4.1.28}$$

Note that all the above equations are for the SI system, i.e. $[d_{\mathrm{eff}}] = \mathrm{m/V}$; $[P] = \mathrm{W}$; $[L] = \mathrm{m}$; $[\lambda] = \mathrm{m}$; $[A] = \mathrm{m}^2$; $\varepsilon_0 = 8.854 \times 10^{-12}\ \mathrm{A\,s/(V\,m)}$; $c = 3 \times 10^8\ \mathrm{m/s}$.

When the powers of the mixing waves are almost equal, the conversion efficiency is for THG, $\omega + 2\,\omega = 3\omega$:

$$\eta = \frac{P_{3\omega}}{(P_{2\,\omega} P_\omega)^{\frac{1}{2}}} ; \tag{4.1.29}$$

for FOHG in the case of $\omega + 3\omega = 4\omega$:

$$\eta = \frac{P_{4\omega}}{(P_{3\omega} P_{\omega})^{\frac{1}{2}}} , \tag{4.1.30}$$

or for $2\,\omega + 2\,\omega = 4\omega$:

$$\eta = \frac{P_{4\omega}}{P_{2\,\omega}} ; \tag{4.1.31}$$

for SFG, $\omega_1 + \omega_2 = \omega_3$:

$$\eta = \frac{P_3}{(P_1 P_2)^{\frac{1}{2}}} ; \tag{4.1.32}$$

for DFG, $\omega_1 = \omega_3 - \omega_2$:

$$\eta = \frac{P_1}{(P_2 P_3)^{\frac{1}{2}}} . \tag{4.1.33}$$

In some cases (mentioned additionally) the conversion efficiency is calculated from the power (energy) of fundamental radiation, e.g. for fifth harmonic generation, $\omega + 4\omega = 5\omega$:

$$\eta = \frac{P_{5\omega}}{P_{\omega}} . \tag{4.1.34}$$

Corresponding equations are valid for energy conversion efficiencies by substituting the pulse energy instead of power in the above equations.

The efficiency η in the case of OPO is calculated by the equation

$$\eta = \frac{E_{\mathrm{OPO}}}{E_0} , \tag{4.1.35}$$

where E_{OPO} is the total OPO radiation energy (signal + idler) and E_0 is the energy of the pump radiation. Conversion efficiency can also be determined in terms of *pump depletion*:

$$\eta = 1 - \frac{E_{\mathrm{unc}}}{E_{\mathrm{pump}}} , \tag{4.1.36}$$

where E_{unc} is the energy of unconverted pumping beam after the OPO crystals. Pump depletions are usually significantly greater than the ordinary η values.

The quantum conversion efficiency (for the ratio of converted and mixing quanta) in the case of exact phase-matching ($\Delta\, k = 0$) for sum-frequency generation, $\omega_1 + \omega_2 = \omega_3$, is determined by the following equation (SI system):

$$\eta = \frac{P_3 \lambda_3}{P_1 \lambda_1} = \sin^2 \left(2\,\pi\, d_{\mathrm{eff}}\, L \sqrt{\frac{2 P_2}{\varepsilon_0\, c\, n_1\, n_2\, n_3\, \lambda_1\, \lambda_3\, A}} \right) , \tag{4.1.37}$$

and for difference-frequency generation, $\omega_1 = \omega_3 - \omega_2$:

$$\eta = \frac{P_1 \lambda_1}{P_3 \lambda_3} = \sin^2 \left(2\,\pi\, d_{\mathrm{eff}}\, L \sqrt{\frac{2 P_2}{\varepsilon_0\, c\, n_1\, n_2\, n_3\, \lambda_1\, \lambda_3\, A}} \right) . \tag{4.1.38}$$

In the presence of linear absorption all the above equations for conversion efficiencies should be multiplied by the factor

$$\exp\left(-\alpha L\right) \approx 1 - \alpha L , \tag{4.1.39}$$

where α is the linear absorption coefficient of the crystal.

4.1.2.5.3 SHG in "nonlinear regime" (fundamental wave depletion)

Analytical equation for SHG power conversion efficiency for the case of fundamental power depletion in the plane-wave approximation and for exact phase matching ($\Delta k = 0$) is given below [99Dmi]:

$$\eta = \frac{P_{2\omega}}{P_\omega} = \tanh^2\left(\frac{L}{L_{\mathrm{nl}}}\right) . \tag{4.1.40}$$

In order to calculate

$$L_{\mathrm{nl}} = (\sigma\, a_0)^{-1} \tag{4.1.41}$$

one should determine a_0 [$\mathrm{V\,cm^{-1}}$]:

$$a_0 = \left[\frac{752\, P_\omega}{\pi\, \zeta^2\, n}\right]^{\frac{1}{2}} \tag{4.1.42}$$

from input radiation power P_ω [W] and the characteristic radius of the beam ζ [cm], and the parameter σ [$\mathrm{V^{-1}}$]

$$\sigma = \frac{8\,\pi^2\, d_{\mathrm{eff}}}{n\,\lambda_\omega} ; \tag{4.1.43}$$

where λ_1 is in m, d_{eff} in $\mathrm{mV^{-1}}$.

4.1.3 Selection of data

Literature up to the end of 1998 is compiled in this chapter. Attempts were made to select the most reliable and recent data.

Tables in Sect. 4.1.4–4.1.8 present data on second, third, fourth, fifth, and sixth harmonic generation of Nd:YAG laser (including intracavity and in external resonant cavities), harmonic generation of iodine, ruby, Ti:sapphire, semiconductor, dye, argon, He–Ne, NH_3, CO, and CO_2 lasers, sum-frequency mixing (including up-conversion of IR radiation into the visible), difference-frequency generation, optical parametric oscillation (cw, nanosecond, picosecond, and femtosecond in the UV, visible, near and mid IR regions) and picosecond continuum generation.

Second harmonic generation of Nd:YAG laser was realized with conversion efficiency of $\eta = 80$ % in KDP and KTP, THG with $\eta = 80$ % in KDP, FOHG with $\eta = 80 - 90$ % (calculated from SH) in ADP and KDP, FIHG in KDP, ADP (upon cooling) and BBO and urea (at room temperature). Second harmonic generation of Ti:sapphire laser with $\eta = 75$ % was achieved in LBO, minimum pulse durations for SH were as short as 10–16 fs (BBO, LBO). Third and fourth harmonics of Ti:sapphire laser were generated in BBO, thus covering the range of wavelengths 193–285 nm. Second harmonic of CO_2 laser with $\eta = 50$ % was obtained in $ZnGeP_2$.

Sum-frequency generation (mixing) is used, in particular, for extending the range of generating radiation into the ultraviolet. By use of SFG the shortest wavelengths in VUV were achieved with KB5 crystal (166 nm), LBO (172.7 nm), CBO, CLBO (185 nm), BBO, KDP and ADP (189, 190, and 208 nm, respectively). At present, $\lambda = 166$ nm is the minimum wavelength achieved by frequency conversion in crystals. Sum-frequency generation is also used for up-conversion of near IR (1–5 μm) and CO_2 laser radiation into the visible. Maximum conversion efficiencies up to 40–60 % were obtained for the latter case in $AgGaS_2$, CdSe, and $HgGa_2S_4$ crystals.

Difference-frequency generation makes it possible to produce IR radiation in the near IR (up to 7.7 μm, in $LiIO_3$), mid IR (up to 18–23 μm, in $AgGaSe_2$, GaSe, CdSe, Ag_3AsS_3) and far IR (0.05–30 mm, in $LiNbO_3$ and GaP).

Optical parametric oscillation is a powerful method for generating continuously tunable radiation in the UV (up to 314–330 nm, in LBO and urea), visible, and IR regions (up to 16–18 μm, in CdSe and GaSe). Singly resonant OPO, or SROPO, uses resonant feedback at only the signal or idler frequency. Doubly resonant OPO, or DROPO, uses resonant feedback of both signal and idler frequencies. Exotic triply resonant OPO, or TROPO, with resonant feedback also at pump frequency, and quadruply resonant OPO, or QROPO, with SHG inside the OPO cavity and resonant feedback also at the second harmonic, are used very seldom.

Different OPO schemes and their energetic, temporal, spectral, and spatial characteristics are considered in detail in [73Zer, 78Dmi, 83Dan, 87Dmi] and in the three special issues of the Journal of the Optical Society of America B (Vol. 10, No. 9 and 11, 1993 and Vol. 12, No. 11, 1995) devoted to optical parametric oscillators. In Tables 4.1.30–4.1.33 we list only the main OPO parameters realized in practice: pump wavelengths, phase-matching angles, pump thresholds (peak intensity and/or average power), tuning ranges, OPO pulse durations, and conversion efficiencies for OPO experiments in the UV, visible, and near IR spectral ranges. The column headed *notes* gives data on the OPO type, pump intensities, crystal lengths, phase-matching temperatures, and output characteristics of OPO radiation (energy, power, bandwidth).

High conversion efficiencies were obtained with resonant schemes of cw OPO ($\eta = 40 - 80$ % with $LiNbO_3$:MgO crystal), nanosecond ($\eta = 60$ % with BBO), traveling-wave and synchronously pumped picosecond OPO ($\eta = 45-75$ % with KDP, KTP, KTA, BBO), and synchronously pumped femtosecond OPO ($\eta = 50$ % with BBO). Minimum pulse durations were 13 fs in SP OPO with BBO crystal, pumped by the second harmonic of a Ti:sapphire laser. Very low power thresholds (0.4 mW) were achieved with $LiNbO_3$:MgO containing quadruply resonant OPO. In general, in the case of OPO the total conversion efficiencies to both, idler and signal wavelengths, are presented. In most cases the conversion efficiency corresponds to the maximum for the range of wavelengths.

The picosecond continuum, first detected in media with cubic nonlinearity (D_2O, H_2O, etc.), was also observed in crystals with square nonlinearity (KDP, $LiIO_3$, $LiNbO_3$, etc.).

We don't pretend to comprehend all directions of frequency conversion in crystals. Some special aspects, e.g. second harmonic generation in layers and films, waveguides and fibers, periodically poled crystals, liquid crystals, as well as different design configurations of frequency converters have been beyond our consideration. For "justification" we refer to Artur L. Schawlow's famous saying: "To do successful research, you don't need to know everything. You just need to know of one thing that isn't known".

4.1.4 Harmonic generation (second, third, fourth, fifth, and sixth)

Table 4.1.5. Second harmonic generation of Nd:YAG laser radiation (1.064 → 0.532 μm).

Crystal	Type of inter-action	θ_{pm} [deg]	I_0 [W cm^{-2}]	τ_p [ns]	L [mm]	Conversion efficiency [%]	Ref.	Notes
KDP	ooe	41	10^9	0.15	25	32 (energy)	[75Att]	
	ooe	41	–	0.05	25	60	[76Att]	
	ooe	41	8×10^9	0.03	14	82 (energy)	[78Mat]	
	ooe	41	7×10^9	0.03	20	81 (energy)	[78Mat]	
	ooe	41.35	–	0.1 ms	40	0.38 (energy)	[93Dim]	$\lambda = 946$ nm
DKDP	eoe	53.5	10^8	18	30	50 (power)	[76Mac]	
	eoe	53.5	3×10^9	0.25	40	70 (power)	[76Mac]	
	eoe	53.5	8×10^7	20	30	50 (energy)	[78Kog]	$P_{2\omega} = 10$ W
	ooe	36.6	3×10^8	8	20	40 (energy)	[91Bor1]	
	eoe	53.7	3×10^8	8	20	50 (energy)	[91Bor1]	
CDA	ooe	90	2×10^8	10	17.5	57 (power)	[74Kat2]	$T = 48$ °C
	ooe	90	4×10^9	0.007	13	25 (energy)	[72Rab]	
DCDA	ooe	90	8×10^7	20	21	40 (energy)	[78Kog]	$T =$ 90 . . . 100 °C
	ooe	90	3×10^8	20	16	40 (energy)	[78Kog]	$P_{2\omega} = 10$ W
	ooe	90	2×10^8	10	13.5	45 (power)	[74Kat2]	$T = 112$ °C
	ooe	90	9×10^7	–	29	50 (power)	[74Amm]	
	ooe	90	–	15	20	57	[76Hon]	$P_{2\omega} = 6$ W
RDA	ooe	50	–	10	–	34 (power)	[75Kat2]	$T = 25$ °C
RDP	ooe	50.8	2×10^8	10	15.3	36 (power)	[74Kat5]	
$LiIO_3$	ooe	30	7×10^7	–	18	44 (power)	[73Dmi]	
	ooe	30	3×10^9	0.04	5	50	[84Van]	
$LiNbO_3$	ooe	90	3.7×10^7	10	20	40	[81Bye]	$T = 120$ °C
	ooe [a]	90			9–30	50	[88Amm]	$P_{2\omega} = 1$ W
LFM	ooe	55.1	2×10^8	–	15	36	[75And]	
KTP	eoe	26 [b]	–	10	–	22	[78Har]	
	eoe	26 [b]	–	0.04	5	18	[83Joh]	
	eoe	25.2 [b]	–	0.07	7.2	52	[85Ale]	
	eoe	25 [b]	2.5×10^8	15	4	60	[85Bel]	
	eoe	30 [b]	2×10^7	35	9	40 (energy)	[86Dri]	multimode
	eoe	30 [b]	9×10^7	35	4	45 (energy)	[86Dri]	multimode
	eoe	30 [b]	10^8	30	5.1	60 (energy)	[86Dri]	two-pass
	eoe	30 [b]	10^8	30	8	50 (energy)	[86Dri]	Gaussian
	eoe	26 [b]	–	0.2	5	55	[87Moo1]	$E_{2\omega} = 0.19$ J
	eoe	23 [b]	2.5×10^8	10	3	30	[86Lav]	
	eoe	23 [b]	3.2×10^8	8.5	4.5	55 (power)	[93Bol]	

(continued)

Table 4.1.5 continued.

Crystal	Type of inter-action	θ_{pm} [deg]	I_0 [W cm^{-2}]	τ_p [ns]	L [mm]	Conversion efficiency [%]	Ref.	Notes
KTP	eoe	–		8	7	80 (energy)	[92Bro]	$E_{2\omega} = 0.72$ J, $T = 55$ °C
	eoe	–	9×10^7	17	10	97 (energy)	[97Coo]	Multistage system with 3 SHG crystals, $E_{2\omega} = 0.2$ J
$KNbO_3$	ooe	19	4.7×10^7	11	4.8	40 (energy)	[92See]	Nd:YLF (1.047 µm)
BBO	ooe	–	1.9×10^8	14	6	47	[87Adh]	$P_{2\omega} = 4.5$ W
	ooe	–	1.67×10^8	14	6	38	[87Adh]	$P_{2\omega} = 8.5$ W
	ooe	–	2.53×10^8	14	6	37	[87Adh]	$P_{2\omega} = 36$ W
	ooe	21	2×10^9	1	6.8	68 (energy)	[86Che]	
	ooe	21	2.5×10^8	8	6.8	58 (energy)	[86Che]	
	ooe	22.8	1.4×10^8	–	7	32 (power)	[90Bha2]	
	ooe	22.8	1.6×10^8	8	7.5	55–60 (energy)	[91Bor1]	
LBO	ooe	0 [b]	10^9	0.035	15	65 (energy)	[91Hua]	$T = 148.5 \pm 0.5$ °C
	ooe	0 [b]	5×10^8	10	12.5	60 (energy)	[90Lin2]	$T = 149$ °C
	ooe	12 [b]	$(5-8) \times 10^8$	9	14	70 (energy)	[91Xie]	
	ooe	12 [b]	1.4×10^8	8	17	55–60 (energy)	[91Bor1]	
CLBO	ooe	29.4	10^{11}	0.0015	7	53 (energy)	[96Sha]	
	type II	41.9	3×10^8	7	12	55 (energy)	[98Yap]	$E_{2\omega} = 1.55$ J

[a] $LiNbO_3$ grown from congruent melt.
[b] φ_{pm}.

Table 4.1.6. Second harmonic generation of Nd:YAG laser radiation in organic crystals.

Crystal	Type of inter-action	d_{eff} / d_{36}(KDP)	θ_{pm} [deg]	φ_{pm} [deg]	η [%]	Ref.	Notes
POM	eeo	13.6	18.1 (1.32 µm)	90	50	[88Jos]	$L = 7$ mm, $\tau_p = 160$ ps
MAP	eoe	38.3	2.2	0	30	[77Oud]	$L = 1$ mm
MAP	oeo	37.7	11	90	40	[77Oud]	$L = 1.7$ mm
mNA	ooe	37.7	90	55	15	[74Dav]	$L = 2.5$ mm, $\Delta\theta = 2.9$ mrad
mNA	ooe	6.8	90	8.5	85	[80Kat3]	NCSHG in the XY plane, $L = 3$ mm
DAN	–	–	40	0	20	[87Nor]	$L = 2$ mm
MHBA	–	30	–	–	59	[93Zha2]	$L = 3$ mm

Table 4.1.7. Intracavity SHG of Nd:YAG laser radiation (1.064 → 0.532 μm).

Crystal	θ_{pm} [deg]	L [mm]	Mode of Nd:YAG laser operation	$P_{2\omega}$ [W]	η [%]	Ref.
$LiIO_3$	29	–	Q-switched	0.3	100	[69Des]
	29	20	cw	4	40 (0.12 [a])	[81Dmi]
	29	–	Continuous pump, mode-locked, $\tau = 800$ ps	5	40 (0.13 [a])	[82Gol]
	29	15	$\tau = 180$ μs, $f = 50$ Hz	100 (peak)	0.06 [a]	[80Koe]
	34	4	Diode-laser pumped cw Nd:YAG laser, $\lambda = 946$ nm	0.52	–	[97Kel]
$LiNbO_3$	90	–	Continuous pump, Q-switched	0.31	100	[72Dmi]
	90	1	$\tau = 60$ ns, $f = 400$ Hz	100 (peak)	–	[68Smi]
Banana	90	3	cw	1.1	100	[68Geu]
	90	–	Continuous pump, Q-switched	0.016	100	[70Che]
	90	5	–	0.3 . . . 0.5	–	[74Gul]
KTP	26	3.5	Q-switched	5.6	–	[84Liu]
	–	4.6	Acoustooptic modulation, $f = 4 \ldots 25$ kHz	28	54 (0.6 [a])	[87Per]
	–	–	Diode-laser pumped cw Nd:YAG laser	0.03 . . . 0.1	6 [a]	[92Ant]
	–	15	Diode-laser pumped mode-locked Nd:YAG laser, $\tau = 120$ ps, $f = 160$ MHz	3	56 (1.3 [a])	[92Mar]
	–	15	Diode-laser pumped cw Nd:YAG laser	2.8	47 (0.94 [a])	[92Mar]
	90	4.4	Q-switched Nd:$YalO_3$ laser, $\lambda = 1.08$ μm	15	–	[86Gar]
	–	5	Diode-laser pumped Nd:YVO_4 laser	0.07	9.1 [a]	[94Tai]
$KNbO_3$	90	5	cw	0.366	90	[77Fuk]
	60	3.7	Diode-laser pumped cw Nd:YAG laser, $\lambda = 946$ nm	0.0031	0.74 [a]	[89Ris]
	0	6.2	Diode-laser pumped cw Nd:YAG laser	0.002	1 [a]	[89Bia]
	90	1.3	Ti-sapphire laser pumped Nd:$YalO_3$ laser, $\lambda = 946$ nm	0.015	–	[95Zar]
BBO	25	4	Diode-laser pumped cw Nd:YAG laser, $\lambda = 946$ nm	0.55	–	[97Kel]
LBO	$\varphi = 11.4$	9	Diode-laser pumped Q-switched Nd:YAG laser, $\tau = 60$ ns	4	10 [a]	[94Han]

[a] Conversion efficiency calculated with respect to the energy of pumping flash lamps or diode lasers.

Table 4.1.8. Second harmonic generation of Nd:YAG laser radiation (1.064 → 0.532 μm) in external resonant cavities.

Crystal	θ_{pm} [deg]	T_{pm} [°C]	L [mm]	Mode of laser operation	$P_{2\omega}$ [W]	η [%]	Ref.
$LiNbO_3$:MgO	90	–	12.5	Diode-laser pumped, cw	0.03	56	[88Koz]
	90	110	12	Diode-laser pumped, cw (monolithic ring frequency doubler)	0.2	65	[91Ger]
	90	107	–	Diode-laser pumped, cw (monolithic ring frequency doubler)	0.005	50	[93Fie]
	90	110	7.5	Diode-laser pumped, cw (monolithic ring frequency doubler)	0.1	82	[94Pas]
$LiNbO_3$	90	233.7	10	Injection-locked Nd:YAG laser	1.6	69	[91Jun]
KTP	90	63	10	cw $YAlO_3$:Nd laser ($\lambda = 1.08$ μm)	0.6	85	[92Ou]
LBO	90 (θ), 0 (φ)	149.5	6	Injection-locked cw Nd:YAG laser	6.5	36	[91Yan]
	90	167	12	Diode-laser pumped mode-locked Nd:YLF laser ($\lambda = 1.047$ μm, $\tau = 12$ ps, $f = 225$ MHz)	0.75	54	[92Mal]

Table 4.1.9. Third harmonic generation of Nd:YAG laser radiation (1.064 → 0.355 μm).

Crystal	Type of inter-action	θ_{pm} [deg]	τ_p [ns]	L [mm]	η [%]	Ref.	Notes
KDP	eoe	58	0.15	12	32 (energy)	[75Att]	$I_0 = 1$ GW cm^{-2}
KDP	eoe [a]	58	25	–	6 (energy)	[79And1]	$P = 40$ MW
KDP	eoe	58	0.05	–	10 (energy)	[72Kun]	
DKDP	eoe	59.5	8	20	17 (energy)	[91Bor1]	$I_0 = 0.25$ GW cm^{-2}
RDA	ooe	66.2	8	14.8	12 (power)	[75Kat2]	$\Delta\theta L = 1.0$ mrad cm
RDP	ooe	61.2	–	15.3	44 (power)	[74Kat5]	$I_0 = 0.2$ GW cm^{-2}
RDP	ooe	61.2	8	15.3	21 (power)	[74Kat1]	
$LiIO_3$	ooe	47	0.8	8	0.7 (power)	[85Bog]	$P_{av} = 4.5$ mW
$LiIO_3$	ooe	47.5	–	4	4 (power)	[71Oka]	
BBO	eoe	64	8	5.5	23 (energy)	[86Che]	$I_0 = 0.25$ GW cm^{-2}
BBO	ooe	31.3	8	7.5	20 (energy)	[91Bor1]	$I_0 = 0.19$ GW cm^{-2}
BBO	ooe	31.3	9	6	35 (quantum)	[93Wu]	Intracavity THG, $P = 0.2$ W
CBO	type II	40.3 [b]	0.035	5	80 [c]	[97Wu]	$I_0 = 5$ GW cm^{-2}
LBO	type I	38.1 [b]	8	12.2	22 (energy)	[91Bor1]	$I_0 = 0.19$ GW cm^{-2}
LBO	type II	41	8	12.6	60 (energy)	[89Wu]	

[a] Neodymium silicate glass laser.
[b] φ_{pm}.
[c] Conversion efficiency from 0.532 μm.

Table 4.1.10. Fourth harmonic generation of Nd:YAG laser radiation (1.064 → 0.266 μm).

Crystal	Type of inter-action	θ_{pm} [deg]	I_0 [W cm^{-2}]	τ_p [ns]	L [mm]	Conversion efficiency (from 532 nm) [%]	Ref.	Notes
KDP	ooe	78	–	7	–	30 . . . 35	[77Aba]	
DKDP	ooe	90	8×10^9	0.03	4	75	[77Rei]	
DKDP	ooe	90	5×10^7	25	20	40	[76Liu]	$T = 60$ °C, $P = 2.5$ MW
DKDP	ooe	90	–	600	50	3.4	[85Per]	$T = 49.8$ °C, $P_{av} = 0.5$ W
ADP	ooe	90	8×10^9	0.03	4	85	[77Rei]	
ADP	ooe	90	–	8	30	15 [a]	[75Kat3]	$T = 51.2$ °C, $P_{av} = 5$ W
BBO	ooe	48	–	5	–	16	[88Lag]	$E = 80$ mJ
BBO	ooe	48	1.6×10^8	1	5	52	[86Che]	
BBO	ooe	57.8	–	80 μs	6.6	0.17	[93Dim]	Nd:YAG laser cooled to 253 K, $\lambda = 946$ nm
CBO [b]	ooe	52.3	4×10^9	0.035	10	60	[97Wu]	
CLBO	ooe	62	–	10	9	30	[95Mor1]	$E = 110$ mJ
CLBO	ooe	61.6	–	7	10	50	[96Yap]	$E = 500$ mJ
CLBO	ooe	62.5	10^{11}	1.5 ps	10	24	[96Sha]	
CLBO	–	–	–	0.014	6	38	[97Sri]	
CLBO	ooe	–	1.7×10^8	46	15	20	[01Koj]	$T = 140$ °C, $P_{av} = 20.5$ W
$Li_2B_4O_7$	ooe	66	–	10	35	20	[97Kom]	$E = 160$ mJ

[a] Efficiency of conversion from 1.064 μm.
[b] $1.064 + 0.355 \rightarrow 0.266$ μm; conversion efficiency from 0.355 μm.

Table 4.1.11. Fifth harmonic (1.064 → 0.2128 μm) and sixth harmonic generation (1.064 → 0.1774 μm) of Nd:YAG laser radiation.

Crystal	θ_{pm} [deg]	Type of interaction	Crystal temperature [°C]	Output parameters	τ_p [ns]	Ref.
KDP	90	ooe [a]	−70	$E = 0.1$ mJ	–	[69Akm]
KDP	90	ooe	−35	$P_{av} = 2.6$ mW, $f = 120$ kHz	30	[78Mas]
KDP	90	ooe	−40	$P_{av} = 2$ mW, $f = 6$ kHz	30	[79Jon]
KDP	84	ooe [b]	20	$E = 0.45$ mJ	0.015	[88Gar, 89Aru]
ADP	90	ooe	−40	$P_{av} = 5 \ldots 7$ mW, $f = 10$ Hz	10	[76Mas1]
ADP	90	ooe [c]	−67.5	$E = 20$ J	0.5	[88Beg]
KB5	$53 \pm 1(\varphi)$	eeo	20	$E = 0.7$ mJ	6	[76Kat1]
KB5	$53 \pm 1(\varphi)$	eeo	20	$E = 0.1$ mJ	0.02	[82Tan]
KB5	$52.1(\varphi)$	eeo	20	$E = 0.3$ mJ	0.03	[80Aru]
Urea	72	eeo	20	$E = 30$ mJ	10	[80Kat1]
BBO	55	ooe	20	$E = 20$ mJ	5	[86Che, 88Lag]
CLBO	–	ooe	20	$E = 35$ mJ	10	[95Mor1]
CLBO	67.3	ooe	20	$E = 230$ mJ	7	[96Yap]
$Li_2B_4O_7$	80	ooe	20	$E = 70$ mJ	10	[97Kom]
KB5 [d]	$90(\theta)$, $68.5(\varphi)$	eeo	20	$P_{av} = 6$ mW	6	[96Ume]
KB5 [d]	$80(\theta)$, $90(\varphi)$	ooe	20		6	[96Ume]

[a] Neodymium silicate glass laser.
[b] Nd:$YAlO_3$ laser.
[c] Nd:YLF laser.
[d] Sixth harmonic generation, $\omega + 5\,\omega = 6\,\omega$.

Table 4.1.12. Generation of harmonics of Nd:YAG laser radiation with $\lambda = 1.318$ μm.

Number of harmonic	λ [nm]	Crystal	θ_{ooe} [deg]	L [mm]	τ_p [ns]	Output parameters	Energy conversion efficiency [%]	Ref.
2	659.4	$LiNbO_3$	44.67	16	40	85 kW	10	[81Akm]
3	439.6	KDP	42.05	30	40	3.4 kW	0.4	[81Akm]
4	329.7	KDP	53.47	30	40	6 kW	0.6	[81Akm]
5 [a]	263.8	KDP	55.33	30	30	0.2 kW	0.02	[81Akm]
6 [b]	219.3	KB5	78 (eeo)	15	45	3 kW	0.5	[87Aru]
2	659.4	DCDA	70.38	13.5	25	1.4 MW	40	[76Kat2]
2 [c]	659.4	$LiIO_3$	22	10	30	1 W (av.)	100	[81Kaz]
2	659.4	$LiNbO_3$	90 ($T = 300$ °C)	19	50	60 mJ	48	[83Kaz]
2	659.4	$LiNbO_3$	90	20	50	10 mJ	21	[83Kaz]
2 [c, d]	659	LBO	$\varphi = 3.7$	–	2	0.3 W (av.)	–	[94Lin]
2 [d]	659	LBO	along Z axis	16	76	0.85 mJ	40	[95Mor2]
3	439.6	KDP	42.05 ($T = 300$ °C)	40	50	1.4 mJ	3	[83Kaz]
3	439.6	$LiIO_3$	–	8	50	1.4 mJ	1.2	[83Kaz]

[a] $\omega + 4\,\omega = 5\,\omega$.
[b] $3\,\omega + 3\,\omega = 6\,\omega$.
[c] Intracavity SHG.
[d] Nd:YLF laser.

Table 4.1.13. Generation of harmonics of high-power Nd:glass laser radiation in KDP crystals.

Fundamental radiation			Second harmonic					Third and fourth harmonics					Ref.
λ [μm]	I_0 [10^9 W cm^{-2}]	τ_p [ns]	λ [μm]	Type of inter-action	η [%]	Crystal length [mm]	E [J]	λ [μm]	Type of inter-action	η [%]	Crystal length [mm]	E [J]	
1.054	2.5	0.14	0.53	eoe [a]	67	12	9	0.35	eoe	80	12	11	[80Sek]
1.054	3.5	0.7	0.53	eoe	67	12	25	0.35	eoe	80	12	30	[80Sek]
1.064	2.5	0.1	0.532	eoe	67	8	17	0.266	ooe	30	7	4	[80Lot]
1.064	9.5	0.7	0.532	ooe	83	10	346						[82Lin]
1.064	2.0	0.7	0.532	eoe	67	12	–	0.355	eoe	55	10	41	[82Lin]
1.064	1.2	0.7	0.532	ooe	–	10	–	0.266	ooe	51	10	50	[82Lin]
1.06	0.2	25	0.53	ooe	80	40	60						[82Ibr]
1.06	2.7	0.5	0.53	ooe	90	30	20						[83Gul]
1.06	2.7	0.5	0.53	eoe [a]	67	18	–	0.35	eoe	81	18	10 . . . 20	[83Gul]
1.053	1.5	0.6	0.53	eoe	70	16	80	0.26	ooe	46	7	53	[85Bru]
1.054	5	0.5	0.53	eoe	87	17.5	–	0.264	ooe	92 [b]	10	–	[88Beg]

[a] The angle between the polarization vector of the fundamental radiation and o-ray is 35 °.
[b] Conversion efficiency from 0.527 μm.

Table 4.1.14. Generation of harmonics of iodine laser radiation: $\lambda = 1.315$ μm ($\tau_p = 1$ ns) [80Fil, 81Wit, 83Fil, 83Bre].

	SHG $\omega + \omega = 2\omega$			THG $\omega + 2\omega = 3\omega$		FOHG $2\omega + 2\omega = 4\omega$	FIHG $2\omega + 3\omega = 5\omega$	SIHG $3\omega + 3\omega = 6\omega$
Wavelength [nm]	657.6			438.4		328.8	263.0	219.2
Crystal	DKDP	KDP	KDP	DKDP	KDP	KDP	KDP	KB5
Crystal length [mm]	19	20	10	20	10	40	–	10
Type of interaction	eoe	eoe	ooe	eoe [a]	ooe	ooe	ooe	eeo
θ_{pm} [deg]	51.3	61.4	44.3	48	42.2	53.6	74	80.5 (φ_{pm})
Conversion efficiency [%] at								
$I_0 = (1 \ldots 1.5) \times 10^9$ W cm^{-2}	30	16	12	30	6	15	–	–
$I_0 = 3 \times 10^9$ W cm^{-2}	70	–	–	50	–	30	9	3

Table 4.1.15. Second harmonic generation of ruby laser radiation (694.3 → 347.1 nm).

Crystal	Type of inter-action	θ_{pm} [deg]	I_0 [W cm^{-2}]	L [cm]	Power conversion efficiency [%]	Ref.	Notes
RDA	ooe	80.3 (90)	1.5×10^8	1.45	58	[74Kat3]	$T = 20$ °C (90 °C), $L\,\Delta\theta = 4.37$ mrad cm
RDP	ooe	67	1.8×10^8	1.0	37	[74Kat4]	$T = 20$ °C, $L\,\Delta\theta = 2.4$ mrad cm
$LiIO_3$	ooe	52	1.3×10^8	1.1	40	[70Nat]	$L\,\Delta\theta = 0.2$ mrad cm

Table 4.1.16. Harmonic generation of Ti:sapphire (Ti:Al_2O_3) laser radiation.

(a) Second harmonic generation.

Crystal	$\lambda_{2\omega}$ [nm]	τ	θ_{pm} [deg]	L [mm]	Output power $P_{2\omega}$ [mW]	η [%]	Ref.	Notes
KDP	390	150 fs	43	3 ... 40	300	50	[95Kry]	
$LiIO_3$	360 ... 425	1.5 ps	43	10	700	50	[91Neb]	
BBO	360 ... 425	1.5 ps	30	8	450	27	[91Neb]	
BBO	430	54 fs	27.5	0.055	230	75 (5.2 [a])	[92Ell]	ICSHG
BBO	383 ... 407	–	ooe	5	170	7.4 [a]	[93Poi]	ICSHG
BBO	425	16 fs	28	0.1 ... 1	40	–	[95Ash]	
BBO	438	10 fs	26.7; ooe	0.04	3.6	1	[98Ste]	
BBO	400	150 fs	ooe	0.5	150	38	[98Zha]	
LBO	400	150 fs	–	3	130	32	[98Zha]	
LBO	350 ... 450	12 ... 25 ns	90 (θ), 22 ... 40 (φ)	5	25 mJ	30	[91Skr]	
LBO	360 ... 425	1.5 ps	90 (θ), 32 (φ)	8	350	20	[91Neb]	
LBO	410	cw	90 (θ), 31.8 (φ)	10.7	410	21.6	[93Bou]	ERR
LBO	416	14 fs	90 (θ), 29 (φ)	0.1	30	–	[94Bac]	ICSHG
LBO	400	1.5 ps	type I	10	1280	75	[94Wat]	ERR
LBO	398	cw	90 (θ), 31.7 (φ)	8	650	70	[95Zho, 96Zho]	ICSHG
$KNbO_3$	430 ... 470	35 ns	along a axis	7.9	7.8 kW	45 (2 [a])	[90Wu]	ICSHG
$KNbO_3$	430	cw	–	6	650	48	[91Pol]	ERR

[a] Total conversion efficiency from the pump source.

(b) Third harmonic generation: $\omega + 2\omega = 3\omega$.

Crystal	$\lambda_{3\omega}$ [nm]	τ	θ_{pm} [deg]	L [mm]	Output power $P_{3\omega}$ [mW]	η [%]	Ref.	Notes
BBO	240 ... 285	1.8 ps	50, ooe	6.5 ... 12	150	30	[91Neb, 92Neb]	$f = 82$ MHz
LBO	266 ... 283	1 ps	90 (θ), 70 (φ)	7	35	10	[91Neb]	$f = 82$ MHz
BBO	252 ... 267	180 fs	58, eoe	0.3	18	6	[93Rin]	$f = 1$ kHz

(c) Fourth harmonic generation.

Crystal	$\lambda_{4\,\omega}$ [nm]	τ	$\theta_{\rm pm}$ [deg]	L [mm]	Output power $P_{4\,\omega}$ [mW]	η [%]	Ref.	Notes
BBO [a]	205 ... 213	1 ps	ooe	8	10	4	[91Neb]	$f = 82$ MHz
BBO [b]	193 ... 210	1 ... 2 ps	75, ooe	6.9	10	4	[92Neb]	$f = 82$ MHz
BBO [b]	193 ... 210	165 fs	65, ooe	0.1	6	3	[98Rot]	$f = 82$ MHz
BBO [b]	193 ... 210	340 fs	65, ooe	0.3	15	–	[98Rot]	$f = 82$ MHz
BBO [b]	189 ... 200	180 fs	71, ooe	0.1	4	1	[93Rin]	NC, $f = 1$ kHz
BBO [b]	186	10 ns	81 (θ), 30 (φ), ooe	5	0.008	–	[99Kou]	$T = 91$ K

[a] $2\,\omega + 2\,\omega = 4\,\omega$.
[b] $\omega + 3\,\omega = 4\,\omega$.

Table 4.1.17. Second harmonic generation of semiconductor laser radiation in $KNbO_3$.

$\lambda_{\,\omega}$ [nm]	Phase-matching conditions	L [mm]	$P_{2\,\omega}$ [mW]	η [%]	Ref.	Notes
842	$T = -23$ °C	5	24	14	[89Gol]	external resonator
865	along a axis	5	0.215	1.7	[89Dix]	External Ring Resonator (ERR)
842	along a axis	5	6.7	0.57	[90Hem]	ERR, cw
856	along a axis, $T = 15$ °C	7	41	39	[90Koz]	external resonator
972	along b axis	5	1.2	4.8	[92Zim]	distributed Bragg reflection semiconductor laser
858	–	12.4	62	1.1	[93Gol]	
858	–	12.4	80	–	[95Gol]	THG in LBO, 90 (θ), 31.8 (φ); 15 mm, $\lambda = 286$ nm, 0.05 mW
972	along b axis	6.5	156	–	[95Zim]	ERR, FOHG in BBO (14 mm) in ERR, $\lambda = 243$ nm, 2.1 mW
860	along a axis	10	50	60	[97Lod]	
858	along a axis	10	90	–	[98Mat]	FOHG in BBO ($\theta = 71$ °): $\lambda = 214.5$ nm, 0.1 mW

Table 4.1.18. Second harmonic generation of dye laser radiation.

Crystal	$\lambda_{2\,\omega}$ [nm]	Parameters of output radiation (energy, power, pulse duration); conversion efficiency	Ref.	Notes
KDP	267.5–310	0.1 kW (peak), $\eta = 1$ %	[76Str]	
KDP	280–310	50 mJ	[77Hir]	
KDP	280	90 mW, $\eta = 10$ %	[95Nie]	$L = 55$ mm, external cavity
ADP	280–310	50 mJ, $\eta = 8.4$ %	[77Hir]	
ADP [a]	290–315	up to 1 mW, $\eta = 0.03$ %	[72Gab]	
ADP [a]	250–260	120 µW	[80Web]	$\theta_{\rm ooe} = 90$ °, $T = 200 \ldots 280$ K
ADP [a]	293	0.13 mW, $\eta = 0.08$ %, $\tau = 3$ ps	[80Yam]	$L = 3$ mm
ADP [a]	295	$\eta = 10^{-4}$, $\tau = 3 \ldots 4$ ps	[80Wel]	$L = 1 \ldots 3$ mm
RDP	313.8–318.5	3.6 MW, $\tau = 8$ ns, $\eta = 52$ % in power	[75Kat1]	$\theta = 90$ °, $T = 20 \ldots 98$ °C, $I_0 = 36$ MW cm^{-2}, $L = 25$ mm
RDP	310–335	3.2 MW, $\tau = 10$ ns, $f = 10$ Hz, $\eta = 36$ %	[77Kat2]	$\theta = 90$ °

(continued)

Table 4.1.18 continued.

Crystal	$\lambda_{2\omega}$ [nm]	Parameters of output radiation (energy, power, pulse duration); conversion efficiency	Ref.	Notes
ADA	292–302	30 mW	[77Fer]	$\theta = 90\,^\circ$
ADA [a]	285–315	400 mW (single-mode regime), 50 mW (multimode regime)	[76Fro]	$\theta = 90\,^\circ$, temperature tuning, $L = 30$ mm
DKDA	310–355	0.8 ... 3.2 MW, $\tau = 10$ ns, $f = 10$ Hz, $\eta = 9 \ldots 36\,\%$	[77Kat2]	$\theta = 90\,^\circ$, $L = 15$ mm
$LiIO_3$ [a]	295	$\eta = 10^{-4}$, $\tau = 2.1$ ps	[80Wel]	$L = 0.3$ mm
$LiIO_3$ [a]	293–312	0.37 mW, cw regime	[86Bue]	$L = 10$ mm
$LiIO_3$	293–330	15 mW, cw regime	[83Maj]	$L = 1$ mm
$LiIO_3$	293	3 kW, $\eta = 30\,\%$	[76Str]	$L = 6$ mm
$LiIO_3$	293–310	4 mW, cw regime, $\eta = 0.4\,\%$	[75Bet]	$L = 6$ mm, $\Delta\lambda = 0.03$ nm
$LiIO_3$	293–310	21 mW, cw regime, $\eta = 2\,\%$	[75Bet]	$L = 6$ mm, $\Delta\nu = 30$ MHz
BBO	204.8–215	100 kW, $\tau = 8$ ns, $\eta = 4 \ldots 17\,\%$	[86Kat]	$\theta = 70\,^\circ \ldots 90\,^\circ$
BBO	205–310	50 kW, $\tau = 9 \ldots 22$ ns, $\eta = 1 \ldots 36\,\%$	[86Miy]	$L = 6$ and 8 mm
BBO [a]	315	20 mW, $\tau = 43$ fs	[88Ede]	$\theta = 38\,^\circ$, $\varphi = 90\,^\circ$, $L = 55$ μm
BBO	230–303	0.02 ... 0.18 mJ, $\tau = 17$ ns	[90Mue]	$\theta_{ooe} = 40 \ldots 60\,^\circ$, $L = 7$ mm
BBO [a]	243	30 mW, cw regime	[91Kal]	$\theta_{ooe} = 55\,^\circ$, $L = 8$ mm, $\Delta\nu = 200$ Hz
KB5	217.3–234.5	0.3 kW, $\tau = 7$ ns, $\eta = 1\,\%$	[75Dew]	XY plane, eeo
KB5	217.1–240	5 ... 6 μJ, $\tau = 3 \ldots 4$ ns, $\eta = 10\,\%$	[76Dew]	XY plane, $\theta_{ooe} = 90 \ldots 0\,^\circ$
KB5	217.1–315.0	5 ... 6 μJ, 5 ns, 10 %	[76Dew]	XY plane, $\varphi_{eeo} = 90 \ldots 31\,^\circ$, $L = 10$ mm
KB5	217–250	0.1 ... 5 μJ, $\eta = 0.2 \ldots 5\,\%$	[76Zac]	XY plane, $\varphi_{eeo} = 90 \ldots 65\,^\circ$
DKB5	216.15	2 μJ, $\tau = 3$ ns, $\eta = 5\,\%$	[78Pai]	$\theta = 90\,^\circ$, $\varphi = 90\,^\circ$
LFM	230–300	$\eta = 2\,\%$	[73Dun]	XZ plane, $\theta_{ooe} = 35 \ldots 45\,^\circ$, $L = 10$ mm
LFM [a]	290–315	$\eta = 10^{-4}$	[72Gab]	XZ plane, $\theta_{ooe} = 45\,^\circ$ (590 nm)
LFM [a]	238–249	70 μJ (244 nm), cw regime	[80Bas]	XZ plane, $\theta_{ooe} = 39\,^\circ$ (486 nm)
LFM	237.5–260	20 W, nanosecond regime, $\eta = 0.7\,\%$	[76Str]	
LFM [a]	243	1.4 mW, cw regime	[84Foo]	$\theta_{ooe} = 36.8\,^\circ$, $L = 15$ mm
LFM	285–310	4 μJ, cw regime	[75Bet]	
$KNbO_3$	425–468	400 kW, $\eta = 43\,\%$	[79Kat]	angular tuning in XY and YZ planes, temperature tuning (20 ... 220 °C) along the a axis
$KNbO_3$	419–475	12 μW, cw regime, $\eta = 0.065\,\%$	[83Bau]	along the a axis, T from −36 °C to +180 °C, $L = 9$ mm
$KNbO_3$ [a]	425–435	21 mW, cw regime, $\eta = 1.1\,\%$	[85Bau]	along the a axis, $T = 0 \ldots 50$ °C, $L = 9$ mm
Urea	238–300	–	[79Hal]	$\theta_{eeo} = 90 \ldots 45\,^\circ$, $L = 2$ mm
Urea	298–370	–	[79Hal]	$\theta_{eoo} = 90 \ldots 50\,^\circ$, $L = 2$ mm

[a] Intracavity SHG.

Table 4.1.19. Second harmonic generation of gas laser radiation.

Type of laser	Crystal	λ [μm]	θ_{pm} [deg]	T [°C]	Ref.
Argon laser	KDP [a]	0.5145	90	−13.7	[67Lab]
	ADP	0.4965	90	−93.2	[73Jai]
	ADP	0.5017	90	−68.4	[73Jai]
	ADP	0.5145	90	−10.2	[73Jai]
	ADP [a]	0.5145	90	−10	[82Ber]
	KB5	0.4579	67.2 (φ_{pm})	20	[76Che]
	KB5	0.4765	60.2 (φ_{pm})	20	[76Che]
	KB5	0.4880	56.6 (φ_{pm})	20	[76Che]
	KB5	0.5145	50.2 (φ_{pm})	20	[76Che]
	BBO	0.5145	49.5	20	[86Xin]
	BBO	0.4965	52.5	20	[86Xin]
	BBO	0.4880	54.5	20	[86Xin]
	BBO	0.4765	57.0	20	[86Xin]
	BBO [a]	0.4880	55	20	[89Zim]
	BBO [a]	0.5145	–	20	[92Tai]
He-Ne laser	$LiIO_3$ [a]	1.152 ... 1.198	25	20	[83Kac]
	$LiNbO_3$	1.152	90	169	[74Ant]
	$LiNbO_3$	1.152	90	281	[75Kus]
	$AgGaS_2$	3.39	33	20	[75Bad]
NH_3 laser	Te	12.8	–	–	[80Sha]
	$CdGeAs_2$	11.7	35.7	–	[87And3]
CO laser	$ZnGeP_2$	5.2 ... 6.3	47.5	–	[87And2]

[a] Intracavity SHG.

Table 4.1.20. Harmonic generation of CO_2 laser radiation.

Crystal	λ [μm]	Nonlinear process	Type of interaction, θ_{pm} [deg]	I_0 [W cm^{-2}]	L [mm]	η (power) [%]	Ref.
Ag_3AsS_3	10.6	SHG	ooe, 22.5	1.1×10^7	4.4	2.2	[75Nik2]
$AgGaSe_2$	10.6	SHG	ooe, 57.5	1.7×10^6	15.3	2.7	[74Bye]
$AgGaSe_2$	10.25	SHG	ooe, 52.7	$< 10^7$	21	35	[85Eck]
$AgGaSe_2$	10.6	SHG	ooe, 53	–	20	0.1 [a]	[97Sto]
$ZnGeP_2$	9.19 ... 9.7; 10.15 ... 10.8	SHG	eeo, 76	–	–	5	[84And]
$ZnGeP_2$	8.6	SHG	eeo, 55.8	–	–	10.1	[87And4]
$ZnGeP_2$	10.6	SHG	eeo, 76	10^9	3	49	[87And1]
$ZnGeP_2$	10.26 ... 10.61	SHG	eeo	4.4×10^7	7.2	11.3	[93Bar2]
$ZnGeP_2$	9.6	SHG	eeo, 70	5.5×10^7	10	8.1	[94Mas]
$ZnGeP_2$	10.78	SHG	eeo, 90	–	10	–	[97Kat]
$CdGeAs_2$	10.6	SHG	oeo, 48.4	1.4×10^7	9	15	[74Kil]
$CdGeAs_2$	10.6	SHG	eeo, 32.5	–	13	21	[76Men]
$CdGeAs_2$	10.6	SHG	eeo, 32.5	–	13	0.44 [a]	[76Men]

(continued)

Table 4.1.20 continued.

Crystal	λ [μm]	Nonlinear process	Type of interaction, θ_{pm} [deg]	I_0 [W cm^{-2}]	L [mm]	η (power) [%]	Ref.
Tl_3AsSe_3	9.6	SHG	–	–	3.7	10.9	[87Pas]
Tl_3AsSe_3	9.6	SHG	ooe, 19	10^7	5 ... 6	28	[89Auy]
Tl_3AsSe_3	10.6	SHG	ooe	6.3×10^8	4.57	57	[91Suh]
Tl_3AsSe_3	9.25	SHG	ooe, 19	2×10^7	46	20	[96Suh]
GaSe	9.3 ... 10.6	SHG	ooe, 12.8 ... 14.4	2×10^7	6.5	9	[89Abd]
GaSe	9.2 ... 11.0	SHG	ooe, 13	–	2.5	–	[95Bha]
$CdGeAs_2$	–	THG	oeo, 45	–	4.5	1.5	[79Men]
Tl_3AsSe_3	9.6	THG	ooe, 21	10^7	5 ... 6	–	[89Auy]
$ZnGeP_2$	10.6	FOHG	eeo, 47.5	–	10	14 [b]	[87And1]
$ZnGeP_2$	–	FOHG	eeo, 47.5	–	5	2	[85And]
$ZnGeP_2$	10.6	FOHG	eeo, 47.8	–	10	–	[97Sto] [a]
$ZnGeP_2$	9.55	FOHG	eeo, 49	–	10	10	[98Cho]
Tl_3AsSe_3	9.6	FOHG	ooe, 27	10^7	5 ... 6	27 [b]	[89Auy]
Tl_3AsSe_3	9.6	FIHG	ooe, 28	10^7	5 ... 6	45 [c]	[89Auy]

[a] Continuous-wave regime.
[b] Conversion efficiency from 2ω.
[c] Conversion efficiency from 4ω.

4.1.5 Sum frequency generation

Table 4.1.21. Sum frequency generation of UV radiation in KDP.

λ_{SF} [nm]	Sources of interacting radiation	τ_p [ns]	Conversion efficiency, power, energy	Ref.
190–212	SRS of 1.064 μm + sum frequency radiation (220–250 nm) [83Tak]	0.02	20–40 μJ	[85Tak]
215–223	2ω of dye laser + Nd:YAG laser	10	10 kW	[76Mas1]
215–245	SRS of 266 nm (4ω of Nd:YAG laser) + OPO (0.9–1.4 μm)	0.02	100 μJ	[83Tak]
217–275	2ω of dye laser + Nd:YAG laser (1.064 μm)	25–30	50–55 %, 10 mW (average)	[83Kop]
217–226	OPO (1.1–1.5 μm) + 4ω of Nd:YAG laser (266 nm)	0.02	100 kW	[82Tan]
218–244	(269–315 nm) [79Ang] + Nd:YAG laser	0.03	0.1 mJ	[79Ang]
239	Nd:YAG laser (1.064 μm) + XeCl laser (308 nm)	0.7	50%	[81Lyu]
240–242	2ω of ruby laser (347 nm) + dye laser	30	1 MW	[78Sti3]
257–320	Dye laser + argon laser	cw regime	0.2 mW	[77Bli]
269–315	SRS of 532 nm (2ω of Nd:YAG laser) + 532 nm	0.03	1–3 mJ	[79Ang]
269–287	OPO (1.29–3.6 μm) + 3ω of Nd:YAG laser (355 nm)	0.02	100 kW	[82Tan]
271	Two copper vapor lasers (511 and 578 nm)	35	1.5%, 100 mW (average)	[89Cou]
288–393 [a]	OPO (0.63–1.5 μm) + 2ω of Nd:YAG laser (0.532 nm)	0.02	100 kW	[82Tan]
360–415	Dye laser + Nd:YAG laser	25–30	60–70%	[79Dud]
362–432	Dye laser + Nd:YAG laser	0.03	20%	[76Moo]

[a] DKDP crystal was used.

Table 4.1.22. Sum frequency generation of UV radiation in ADP.

λ_{SF} [nm]	Sources of interacting radiation	τ_p [ns]	Conversion efficiency, power, energy	Ref.
208–214	2ω of dye laser + Nd:YAG laser, $\theta = 90\,^\circ$, $T = -120\,^\circ \ldots 0\,^\circ$C	10	1.7 μJ	[76Mas1]
222–235	2ω of dye laser + Nd:YAG laser	10	10%	[76Mas1]
240–248	Dye laser + 2ω of ruby laser, $\theta = 90\,^\circ$, $T = -20 \ldots +80\,^\circ$C	30	4%, 1 MW	[78Sti3]
243–247 [a]	Dye laser + argon laser (363.8 nm)	cw regime	4 mW	[91Kal, 83Cou]
243 [a]	Dye laser + argon laser (351 nm), $\theta = 90\,^\circ$, $T = 8\,^\circ$C	cw regime	0.3 mW	[83Hem1]
247.5	Dye laser + krypton laser (413.1 nm), $\theta = 90\,^\circ$, $T = -103\,^\circ$C	cw regime	–	[79Mar]
246–259	Dye laser + 2ω of Nd:YAG laser, $\theta = 90\,^\circ$, $T = -120 \ldots 0\,^\circ$C	10	1%, 3 μJ	[76Mas1]
252–268 [a]	Dye laser + argon laser (477, 488, 497 nm), $\theta_{ooe} = 90\,^\circ$	cw regime	8 mW	[82Liu]
270–307	Dye laser + 2ω of Nd:YAG laser, $\theta_{ooe} = 81\,^\circ$	ps regime	–	[76Moo]

[a] ADP crystal was placed in an external resonator.

Table 4.1.23. Sum frequency generation of UV radiation in BBO.

λ_{SF} [nm]	Sources of interacting radiation	τ_p [ns]	Conversion efficiency, power, energy	Ref.
188.9–197	Dye laser (780–950 nm) + 2ω of another dye laser (248.5 nm)	10	up to 0.1 mJ	[88Mue]
190.8–196.1	Ti:sapphire laser (738–825 nm) + 2ω of Ar laser (257 nm)	–	tens of nW	[91Wat]
193	Dye laser + KrF laser (248.5 nm)	9	0.2 %, 2 μJ	[88Mue]
193	Dye laser (707 nm) + 4ω of Nd:YAG laser	90–250 fs	10 μJ (250 fs)	[92Hof]
193.3	Dye laser (724 nm, 5 ps) + 4ω of Nd:YLF laser (263 nm, 25 ps)	0.01	1.7 %, 4 μJ (2.5 mJ) [a]	[92Tom]
193.4	FOHG of dye laser radiation (774 nm, 300 fs), $\omega + 3\omega = 4\omega$	800 fs	0.5 μJ (1.5 mJ) [a]	[92Rin]
194	Ti:sapphire laser + 2ω of Ar laser (257 nm), three crystal configuration with external cavity	–	0.016 mJ	[92Wat]
194	Diode laser (792 nm) + 2ω of Ar laser (257 nm)	cw	2 mW	[97Ber]
195.3	THG of dye laser (T [crystal] = 95 K)	17	5 %, 8 μJ	[88Lok]
196–205	Dye laser + 2ω of another dye laser	5	0.1 mJ	[92Hei]
197.7–202	THG of dye laser	0.008	1 %, 1–4 mW	[88Gus]
198–204	THG of dye laser	5	20 %, 1.7 mJ	[87Gla]
271	Two copper vapor lasers (511 and 578 nm)	35	0.9 %, 64 mW	[89Cou]
362.6–436.4	Dye laser + Nd:YAG laser, noncollinear SFG (NCSFG), $\alpha = 4.8 \ldots 21.3\,^\circ$	–	1 %, 0.065 mJ	[90Bha1]
369	Diode laser (1310 nm) + Ar laser (515 nm)	–	1.3 μW	[91Sug]
370.6	Dye laser (568.6 nm) + Nd:YAG laser, NCSFG, $\alpha = 6.3\,^\circ$	–	8–18%	[92Bha]

[a] After amplification in an ArF excimer gain module.

Table 4.1.24. Sum frequency generation of UV radiation in LBO.

λ_{SF} [nm]	Sources of interacting radiation	τ_p [ns]	Conversion efficiency, power, energy	Ref.
170–185 [a]	OPO (1.6–2.5 μm) + 4 ω of Ti-sapphire laser (189–210 nm), θ = 66–90 °, ooe	100 fs	4	[98Pet3]
172.7–187	OPO (1.65–2.15 μm) + 4 ω of Ti-sapphire laser (190–203.75 nm), θ = 90 °, φ = 73 °, ooe	130 fs	50 nJ	[94Sei3]
185–187.5 [b]	OPO + 5 ω of Nd:YAG laser (212.8 nm), θ = 62–74 °	–	–	[95Kat]
194 [b]	OPO + 5 ω of Nd:YAG laser (212.8 nm), θ = 51.2 °, φ = 90 °	5	2.2 %	[00Kag]
185 [c]	OPO + 5 ω of Nd:YAG laser (212.8 nm), θ = 64 °	–	–	[97Ume]
194 [c]	OPO + 5 ω of Nd:YAG laser (212.8 nm), θ = 53 °, φ = 0 °	5	1 %	[00Kag]
195–210 [c]	Nd:YAG laser + 2 ω of dye laser,	10	14 %	[00Bha]
226–265	2 ω or 3 ω of dye laser			
188–195	OPO (1.6–2.3 μm) + 5 ω of Nd:YAG laser (212.8 nm), θ = 90 °, φ = 90–52 °, ooe	6	0.2–2 %, 2–40 μJ	[91Bor2]
187.7–195.2	OPO (1.591–2.394 μm) + 5 ω of Nd:YAG laser, θ = 90 °, φ = 88–50°, ooe	8	3 kW (peak)	[92Wu]
191.4	SRS in H_2 (1.908 μm) + 5 ω of Nd:YAG laser, θ = 90 °, φ = 88–50°, ooe	8	10 %, 67 kW (peak), 2 mW (average)	[92Wu]
218–242	OPO (1.2–2.6 μm) + 4 ω of Nd:YAG laser (266 nm), θ = 90 °, φ = 90–33°, ooe	6	0.2–2 %, 20–400 μJ	[91Bor2]
232.5–238	Nd:YAG laser + 2 ω of dye laser	10	–	[90Kat]
240–255	Nd:YAG laser + 2 ω of dye laser, NCSFG	10	8 %, 0.12 mJ	[93Bha]

[a] $Li_2B_4O_7$ crystal was used.
[b] CBO crystal was used.
[c] CLBO crystal was used.

Table 4.1.25. Sum frequency generation of UV radiation in KB5.

λ_{SF} [nm]	Sources of interacting radiation	τ_p [ns]	Conversion efficiency, power, energy	Ref.
208–217	Two dye lasers, θ = 90 °, φ = 90 °, eeo	10	0.025 %, 1 W	[76Dun]
196.6	Dye laser + 2 ω of Nd:YAG	8	0.1 %, 0.5 mJ	[77Kat1]
207.3–217.4	Ruby laser (694.3 nm) + 2 ω of dye laser	3	0.3 %, 0.8 mJ	[77Kat2]
201–212	Nd:YAG + 2 ω of dye laser	20	10 %, 2–10 μJ	[77Sti]
185–200	Dye laser (740–910 nm) + 2 ω of dye laser (237 nm), θ = 90 °, eeo	30	10 %, up to 10 μJ	[78Sti2]
211–216	Dye laser + Ar laser (351.1 nm)	cw regime	10^{-6}, 50–100 nW	[78Sti1]
196.7–226	OPO + 3 ω and 4 ω of Nd:YAG laser, θ = 90 °, φ = 65 °, eeo	0.02	20 kW	[82Tan]
194.1–194.3	Dye laser + 2 ω of Ar laser (257 nm)	cw regime	2 μW	[83Hem2]
200–222	OPO + 3 ω and 4 ω of Nd:YAG laser	0.045	2×10^{-5}, 1 μJ	[83Pet]
166–172	OPO (1.15–1.6 μm) + 4 ω of Ti-sapphire laser, θ = 90 °, φ = 90 °, eeo	200 fs	0.05–0.4 MW	[98Pet2]

Table 4.1.26. Up-conversion of near IR radiation into the visible.

Crystal	λ_{IR} [μm]	Pump source	η [%]	Ref.
$LiIO_3$	3.39	0.694 μm, mode-locked ruby laser	100	[73Gur]
	3.2 ... 5	1.064 μm, Nd:YAG laser	0.001	[74Gur]
	2.38	0.488 μm, argon laser	4×10^{-8}	[75Mal2]
	1.98, 2.22, 2.67	0.694 μm, mode-locked ruby laser	0.14 ... 0.28	[75Mal1]
	3.39	0.5145 μm, argon laser	2.4×10^{-2}	[80See]
	1 ... 2	0.694 μm, ruby laser	18	[71Cam]
$LiNbO_3$	1.69 ... 1.71	0.694 μm, Q-switched ruby laser	1	[67Mid]
	1.6 ... 3.0	0.694 μm, Q-switched ruby laser	100	[75Aru]
	1.6	0.694 μm, ruby laser	10^{-5}	[68Mid]
	3.3913	0.633 μm, cw He-Ne laser	10^{-5}	[67Mil]
	3.3922	0.633 μm, cw He-Ne laser	5×10^{-5}	[73Bai]
KTP	1.064	0.809 μm, diode laser	68	[93Kea]
	1.54	0.78 μm, diode laser	7×10^{-4}	[93Wan1]
	1.064	0.824 μm, dye laser (intracavity SFG)	0.26	[90Ben]
	1.064	0.809 μm, diode laser	55	[92Ris]
	1.064	0.805 μm, diode laser	24	[92Kea]
	1.319; 1.338	0.532 μm, 2ω of Q-switched Nd:YAG laser	10	[89Sto]

[a] The angle between the polarization vector of the fundamental radiation and o-ray is 35 °.

Table 4.1.27. Up-conversion of CO_2 laser radiation by sum-frequency generation.

Crystal	Pump source	λ_{pump} [μm]	Type of interaction	θ_{pm} [deg]	I_0 [W cm^{-2}]	L [mm]	η [%]	Ref.
Ag_3AsS_3	ns Nd:YAG laser, 740 W	1.064	eoe	20	–	6	0.84	[72Tse]
	Ruby laser, 1 ms	0.694	–	–	10^4	10	0.14	[72Luc]
	ns Nd:YAG laser	1.064	eoe	20	400	6	0.5	[73Alc]
	Nd:YAG laser	1.064	eoe	20	–	14	1.5	[74Vor]
	Ruby laser, 25 ps	0.694	ooe	25.2	10^8	5	10.7	[75Nik1]
	ns Nd:YAG laser	1.064	eoe	20	–	–	30 [a]	[79Jaa]
	ns Nd:YAG laser	1.064	eoe	20	$(0.5 \ldots 1.2) \times 10^6$	–	8 [b]	[81And]
$AgGaS_2$	Nd:YAG laser	1.064	oee	40	6×10^5	3	40 [a]	[75Vor]
	Dye laser, 3 ns	0.598	ooe	90	–	5	40	[77Jan]
	Ruby laser, 30 ns	0.694	eoe	55	–	3.3	9	[77And1]
	ns Nd:YAG laser	1.064	oee	40	–	–	30	[78Vor]
	ns Nd:YAG laser	1.064	oee	40	$(0.5 \ldots 1.2) \times 10^6$	–	14 [b]	[81And]
$HgGa_2S_4$	ns Nd:YAG laser	1.064	ooe	41.6	$(0.5 \ldots 1.2) \times 10^6$	3.6	60 (20) [b]	[80And, 81And]
$ZnGeP_2$	Nd:YAG laser	1.064	oeo	82 ... 89	–	10	1.4	[71Boy]
	ns Nd:YAG laser	1.064	oeo	82.9	$(0.5 \ldots 1.2) \times 10^6$	–	6 [b]	[81And]
	Nd:YAG laser, 30 ns	1.064	oeo	82.5	3×10^6	3	5	[79And2]
CdSe	Nd:YAG laser	1.833	oeo	77	2.4×10^7	10	35 [a]	[71Her]
	HF laser, 250 ns	2.72	oeo	70.5	6×10^6	30	40	[76Fer]

[a] Power-conversion efficiency.

[b] Power-conversion efficiency for two cascades:
$10.6 + 1.064 \rightarrow 0.967$ μm,
$0.967 + 1.064 \rightarrow 0.507$ μm.

4.1.6 Difference frequency generation

Table 4.1.28. Generation of IR radiation by DFG.

(a) Crystal: $LiIO_3$

λ [μm]	Sources of interacting radiations, crystal parameters	Conversion efficiency, energy, power, τ_p	Ref.
4.1–5.2	Dye laser + ruby laser, ICDFG, $L = 12$ mm	100 W (peak)	[72Mel]
1.25–1.60; 3.40–5.65	Dye laser + Q–switched Nd:YAG laser (1.064 and 0.532 μm), ICDFG, $\theta_{ooe} = 21$–28.5 °	0.5–70 W (peak), $\Delta\nu = 0.1$ cm^{-1}, 60 ns	[75Gol]
2.6–7.7	Dye laser + 2ω of Nd:YAG laser, $\theta_{ooe} = 22$ °	2 nJ–50 μJ, 10 ns	[95Cha2]
2.3–4.6	Dye laser + argon laser (514 and 488 nm)	0.5–4 μW, cw	[76Wel]
4.3–5.3	Dye laser + 2ω of Nd:YAG laser, $\theta_{ooe} = 24.3$ °	–	[77Dob]
0.7–2.2	Dye laser + nitrogen laser, $\theta_{ooe} = 51$–31 °	3 ns	[78Koe]
3.8–6.0	Dye laser + copper vapor laser (511 nm), $\theta_c = 21$–24 °	10–100 μW, 20 ns	[82Ata]
3.5–5.4	Dye laser + 2ω of Nd:YAG laser, $\theta_{ooe} = 20$ °	0.8 mJ, 10 ns	[83Man]
1.2–1.6	Two dye lasers, $\theta_{ooe} = 29$ °	1.5–5 ps	[84Cot]
4.4–5.7	Dye laser + Nd:YAG laser, $\theta_{ooe} = 20$–22 °	550 kW, 8 ns	[85Kat]
∼ 5	Two dye lasers, $\theta_{ooe} = 20$ °, $L = 3$ mm	10 %, 10 nJ, 400 fs	[91Els]
2.5–5.3	Signal and idler pulses of OPO, $\theta_{ooe} = 21$ °	0.2 mW, $f = 82$ MHz, 200 fs	[94Loh]
6.8–7.7	Dye laser + 2ω of Nd:YAG laser, $\theta = 28$–29 °	100 mW (peak)	[95Cha1]

(b) Crystal: $LiNbO_3$

λ [μm]	Sources of interacting radiations, crystal parameters	Conversion efficiency, energy, power, τ_p	Ref.
3–4	Dye laser + ruby laser	1 %, 6 kW	[71Dew]
2.2–4.2	Dye laser + argon laser	1 μW, cw	[74Pin]
2–4.5	Dye laser (1.2 ps) + argon laser (100 ps), $\theta = 90$ °, $T = 200 \ldots 400$ °C	25 μW (average), 1.2 ps, $f = 138$ MHz	[84Rud, 85Ree]
2–4	Dye laser + Nd:YAG laser, $\theta_{ooe} = 46 \ldots 57$ °	60 %, 1.6 MW	[80Kat2]
2.04	Two dye lasers, $\theta_{ooe} = 90$ °	50 %, $\Delta\lambda = 0.03$ nm	[77Sey]
1.7–4.0	CPM dye laser + subpicosecond continuum, $\theta_c = 55$ °, $L = 1$ mm	10 kW (peak), 0.2 ps, $\Delta\nu = 100$ cm^{-1}	[87Moo2]
4.043	Two Nd:YAG lasers (1.064 and 1.444 μm), $L = 25$ mm	5.5 %, 30 mJ, 14 ns	[94Won]
1.6–4.8	Nd:glass laser + OPO	6 %, 30 μJ, 1–3 ps	[95DiT]

(c) Crystal: BBO

λ [μm]	Sources of interacting radiations, crystal parameters	Conversion efficiency, energy, power, τ_p	Ref.
2.5	Dye laser (620 nm) + picosecond continuum (825 nm), $\theta_{ooe} = 20.3$ °, $L = 5$ mm	5 %, 4 μJ, 0.5 ps	[91Pla]
0.9–1.5	Dye laser + Nd:YAG laser, $\theta_{ooe} = 20.5$–24.5 °, $L = 10$ mm	23 %, 4.5 mJ, 8 ns	[93Ash]
2.04–3.42	Two dye lasers, NCDFG, $\theta_{ooe} = 12$–17 °, $L = 6$ mm	300–400 W (peak)	[91Bha]
1.23–1.76	Dye laser + Ti:sapphire laser	10 μW (average), 150 fs, $f = 80$ MHz	[93Sei]

(d) Crystal: KTP

λ [μm]	Sources of interacting radiations, crystal parameters	Conversion efficiency, energy, power, τ_p	Ref.
1.4–1.6	Dye laser + Nd:YAG laser, $\theta_{eoe} = 76$–$78\,^\circ$, $\varphi = 0\,^\circ$	8.4 kW, $f = 76$ MHz, 94 fs	[75Bri]
1.35–1.75	Dye laser + $2\,\omega$ of Ti:sapphire laser, ICDFG	10 W (peak), 1.6 ps	[94Pet]
2.8–3.6	Ti:sapphire laser + OPO, $\theta_{eoe} = 90\,^\circ$, $\varphi = 47\,^\circ$	40–150 μW, 90–350 fs, $f = 82$ MHz	[95Gal1]
1.2–2.2	Nd:YAG laser + dye laser, $\theta_{eoe} = 90\,^\circ$, $\varphi = 31\,^\circ$	36 % (quantum), 1 mJ	[95Cha3]
1.05–2.8	Two Ti:sapphire lasers, dye laser + Ti:sapphire laser	20 μW, cw	[96Mom]
1.14–1.23	Dye laser (550–570 nm) + Nd:YAG laser, $\theta_{eeo} = 82$–$90\,^\circ$, $\varphi = 0\,^\circ$	22 % (quantum), 3.3 mJ	[96Bha]

(e) Crystal: KTA

λ [μm]	Sources of interacting radiations, crystal parameters	Conversion efficiency, energy, power, τ_p	Ref.
2.66–5.25	Ti:sapphire laser + Nd:YAG laser, $\theta_{eoe} = 40\,^\circ$, $\varphi = 0\,^\circ$	60 % (quantum), 1–15 mJ, 2 ns	[95Kun]

(f) Crystal: Ag_3AsS_3

λ [μm]	Sources of interacting radiations, crystal parameters	Conversion efficiency, energy, power, τ_p	Ref.
11–23	Two dye lasers	3 W (peak), 30 ns	[76Hoc]
3.7–10.2	OPO (1.06–1.67 μm) + $2\,\omega$ of phosphate glass laser (527 nm)	25–50 μJ, 10 ps	[80Bar1]

(g) Crystal: $AgGaS_2$

λ [μm]	Sources of interacting radiations, crystal parameters	Conversion efficiency, energy, power, τ_p	Ref.
5.5–18.3	Two dye lasers, $\theta = 90\,^\circ$	4 W, 4 ns	[76Sey]
5–11	Dye laser + Nd:YAG laser, $\theta_{eoe} = 38$–$52\,^\circ$	180 kW, 12 ns	[84Kat]
3.9–9.4	Dye laser + Nd:YAG laser	1 %, 8 ps	[85Els]
4–11	OPO (2–4 μm) + radiation at $\lambda = 1.4$–2.13 μm	1 kW, 8 ns	[86Bet]
8.7–11.6	Two dye lasers, $\theta_{ooe} = 65$–$85\,^\circ$	0.1 mW, 500 ns	[74Han]
4.6–12	Two dye lasers, $\theta_{ooe} = 45$–$83\,^\circ$	300 mW, 10 ns	[73Han]
7–9	Dye laser + Ti:sapphire laser, $\theta_{ooe} = 90\,^\circ$	1 μW, cw, $\Delta\,\nu = 0.5$ MHz	[92Can]
4.76–6.45	Dye laser + Ti:sapphire laser, $\theta_{ooe} = 90\,^\circ$, $L = 45$ mm	20 μW, cw, $\Delta\,\nu = 1$ MHz	[92Hie]
~ 4.26	GaAlAs laser (858 nm) + Ti:sapphire laser (715 nm), $\theta_{ooe} = 90\,^\circ$	47 μW (cw), 89 μW (50 μs)	[93Sim2]
4.73; 5.12	Diode laser + Ti:sapphire laser, $\theta_{ooe} = 90\,^\circ$	1 μW, cw	[93Sim1]
5.2–6.4	Nd:YAG laser + near IR (DFG in $LiIO_3$)	35 %, 23 ps	[88Spe]
3.4–7.0	Dye laser + Nd:YAG laser, $\theta_c = 53.2\,^\circ$	17 μW (average), 2.16 ps, $f = 76$ MHz	[91Yod]
4–10	Dye laser (1.1–1.4 μm) + Nd:glass laser (1.053 μm)	2 %, 10 nJ ... 1 μJ, 1 ps	[93Dah]

(continued)

Table 4.1.28 (g) continued.

λ [μm]	Sources of interacting radiations, crystal parameters	Conversion efficiency, energy, power, τ_p	Ref.
4.5–11.5	Dye laser (870–1000 nm) + Ti:sapphire laser (815 nm), $\theta_c = 45\,^\circ$, $L = 1$ mm	10 nJ, $f = 1$ kHz, 400 fs	[93Ham]
9	Ti:sapphire laser with dual wavelength output (50–70 fs), $\theta_c = 44\,^\circ$, $L = 1$ mm	0.03 pJ, $f = 85$ MHz	[93Bar1]
3.1–4.4	Ti:sapphire laser + Nd:YAG laser, ICDFG, $\theta_c = 74\,^\circ$	0.3 mW, cw	[95Can]
2.5–5.5	Signal and idler pulses of OPO, $\theta = 40\,^\circ$	0.5 mW, $f = 82$ MHz, 200 fs	[94Loh]
6.2–9.7	Two Ti:sapphire lasers (696–804 nm and 766–910 nm)	3 μJ, 0.08 %, 13 ns	[96Aka]
6.8–12.5	Two diode lasers (766–786 nm and 830–868 nm)	1 μW, cw	[98Pet1]
2.4–12	Signal and idler waves of BBO based OPA	2.5 mW, 50 fs	[98Gol]
5–12	Signal and idler waves of $LiNbO_3$ based OPO (1.8–2.7 μm)	0.1 mJ, 6 ns	[99Hai]
~ 5	Two diode lasers, $\theta = 90\,^\circ$, $L = 30$ mm	0.2 μW, cw	[96Sch]

(h) Crystal: $AgGaSe_2$

λ [μm]	Sources of interacting radiations, crystal parameters	Conversion efficiency, energy, power, τ_p	Ref.
7–15	OPO (1.5–1.7 μm) + Nd:YAG laser (1.32 μm), $\theta_{ooe} = 90$–$57\,^\circ$	1.2 %	[74Bye]
12.2–13	CO laser (5.67–5.85 μm) + CO_2 laser, $\theta = 61\,^\circ$	0.2 μW, cw	[73Kil]
8–18	Idler and signal waves of OPO	0.1 mJ, 3–6 ns	[93Bos]
5–18	Idler and signal waves of OPO, $\theta_{ooe} = 51\,^\circ$	0.2 mJ, 8 ns	[98Abe]

(i) Crystal: $CdGeAs_2$

λ [μm]	Sources of interacting radiations, crystal parameters	Conversion efficiency, energy, power, τ_p	Ref.
11.4–16.8	CO laser + CO_2 laser	4 μW, cw	[74Kil]

(j) Crystal: GaSe

λ [μm]	Sources of interacting radiations, crystal parameters	Conversion efficiency, energy, power, τ_p	Ref.
9.5–18	Dye laser + ruby laser	300 W, 20 ns	[76Abd]
4–12	Idler and signal waves of OPO	60 W	[78Bia]
7–16	Nd:YAG laser + laser on F_{2^-} colour centers, $\theta_{ooe} = 13$–$15\,^\circ$, $\theta_{eoe} = 12$–$16\,^\circ$	0.1–1 kW, 10 ns	[80Gus]
6–18	Dye laser (1.1–1.4 μm) + Nd:glass laser (1.053 μm)	10 nJ . . . 1 μJ, 1 ps	[93Dah]
5.2–18	Idler and signal waves of OPO, $L = 1$ mm	2 mW, 3.3 %, $f = 76$ MHz, 120 fs	[98Ehr]

(k) Crystal: CdSe

λ [μm]	Sources of interacting radiations, crystal parameters	Conversion efficiency, energy, power, τ_p	Ref.
16	OPO signal wave (1.995 μm) + OPO idler wave (2.28 μm), $\theta = 62.22\,^\circ$	0.5 kW, 20 Hz, 10 ns	[77And2]
9–22	OPO (2–4 μm) + radiation at $\lambda = 1.4$–2.13 μm	10–100 W, 8 ns	[86Bet]
10–20	OPO signal and idler waves, $\theta = 70\,^\circ$, eoo	50 % (quantum), 5–40 μJ, 10 ps	[95Dhi]

(l) Crystal: Te

λ [μm]	Sources of interacting radiations, crystal parameters	Conversion efficiency, energy, power, τ_p	Ref.
10.9–11.1	CO_2 laser (10.2 μm) + cw spin-flip laser (5.3 μm), $\theta_{eeo} = 14\,^\circ$	10 μW	[75Bri]

Table 4.1.29. Difference frequency generation in the far IR region.

Pump sources	Crystal	ν [cm^{-1}]	λ [mm]	Power, energy	Ref.
Nd:glass (1.06 μm)	$LiNbO_3$	100	0.1	–	[65Zer]
Ruby laser (0.694 μm)	$LiNbO_3$	29	0.33	–	[69Yaj]
Two ruby lasers (0.694 μm), 1 MW, 30 ns	Quartz, $LiNbO_3$	1.2–8.0	1.25–8.33	20 mW	[69Far]
Nd:glass (1.06 μm), 50 mJ, 10 ps	ZnTe, $LiNbO_3$	8–30	0.33–1.25	20 mW/cm^{-1}	[71Yaj]
Nd:glass (1.06 μm), 10 ps	$LiIO_3$	–	–	–	[72Tak]
Dye laser (0.73–0.93 μm), 11–15 ns, 4–13 MW	ZnTe, ZnSe, $LiNbO_3$	5–30	0.33–2.00	1 W (ZnTe)	[73Mat]
Nd:glass (1.064 μm), 10 ps	$LiNbO_3$	0.4–2.5	4–25	60 W	[76Ave]
Two ruby lasers (0.694 μm), 20 ns	$LiNbO_3$	1–3.3	3–10	0.5 W	[79Ave]
Ruby laser (0.694 μm)	$LiNbO_3$	1.67–3.3	3–6	–	[80Mak]
Two dye lasers: $\tau_1 = 1$–2 ps, $\lambda_1 = 589$ nm, $E_1 = 0.2$ mJ; $\tau_2 = 20$ ns, $\lambda_2 = 590$–596 nm, $E_2 = 20$ mJ	$LiNbO_3$	20–200	0.05–0.5	3 nJ	[85Ber]
Nd:YAG laser (45 ps) + OPO (35 ps)	$LiNbO_3$	10–200	0.05–1	10 kW	[95Qiu]
CO_2 laser at two frequencies	GaAs	2–100	0.1–5.0	–	[85Rya]
Two CO_2 lasers	$ZnGeP_2$	70–110	0.09–0.14	1.7 μW	[72Boy]
Two CO_2 lasers	$ZnGeP_2$	99–100	0.1–0.11	3.6 μJ	[96Apo]
Nd:YAG (1.064 μm), 30 ns	GaP	0.33–1	10–30	1 mW	[87Len]

4.1.7 Optical parametric oscillation

Table 4.1.30. Continuous wave (cw) and nanosecond OPO in the UV, visible, and near IR regions.

Crystal	θ_{pm}, type of interaction	λ_{pump} [μm]	I_{thr} [MW cm^{-2}]	λ_{OPO} [μm]	τ_p [ns]	η [%]	Ref.	Notes
KDP	eoe	0.532	1000–2000	–	–	40–42 [a]	[86Bar]	TWOPO, $L_1 = 4$ cm, $L_2 = 6$ cm, $E = 2$ J
	eoe	0.35	1000	0.45–0.6	0.5	41 [a]	[87Beg]	TWOPO, $L_1 = 2$ cm, $L_2 = 6$ cm, $E = 0.35$ J, $I_0 = 6$–8 GW cm^{-2}
ADP	–	0.527	1500	0.93–1.21	–	37 [a]	[84Akh]	TWOPO, $E = 2.3$ J, $I_0 = 10$ GW cm^{-2}
	ooe	0.266	–	0.42–0.73	2	25	[71Yar]	TWOPO, $T = 50$–105 °C
	ooe	0.266	250	–	14	30	[75Zhd]	$L = 6$ cm, $I_0 = 1$ GW cm^{-2}
$LiIO_3$	$\theta_{ooe} = 24$ °	1.06	50	2.5–3.2	40	15	[84Ash]	SROPO, $L = 6$ cm, $E = 0.1$ J
	$\theta_{ooe} = 23.1$–22.4 °	0.694	5	1.15–1.9	20	50 [a]	[71Cam, 72Cam]	DROPO, $L = 0.85$ cm, $P = 10$ kW
	$\theta_{ooe} = 25$–30 °	0.53	10	0.68–2.4	15	8	[70Izr]	SROPO, $L = 1.6$ cm
	$\theta_{ooe} = 23$–30 °	0.532	10	0.63–3.35	30	20	[77Dzh]	SROPO
$LiNbO_3$	$\theta_{ooe} = 90$ °	1.06	–	2.13	100	8	[69Amm]	DROPO, $L = 3$ mm
	$\theta_{ooe} = 90$ °	1.06	–	1.4–4.45	20	15	[74Her]	SROPO, $I_0 = 10$ MW cm^{-2}
	43.3 °	0.93	8 mJ	1.48–1.8; 1.95–2.55	16	9.7	[97Raf]	SROPO, $L = 50$ mm, broad spectral bandwidth ($\Delta\lambda = 320$ nm)
	$\theta_{ooe} = 90$ °	0.473–0.659	–	0.55–3.65	130–700	46 (67[a])	[70Wal]	SROPO, $T = 110$–430 °C, $P_{av} = 105$ mW
$LiNbO_3$:MgO	$\theta_{ooe} = 90$ °	1.06	0.4 mW	1–1.14	cw	–	[93Sch]	Quadruply resonant OPO
	$\theta_{ooe} = 90$ °	0.532	35 mW	1.01–1.13	cw	40 (60[a])	[89Koz]	DROPO, $T = 107$–110 °C
	$\theta_{ooe} = 90$ °	0.532	12 mW	1.007–1.129	cw	34 (78[a])	[89Nab]	DROPO, $T = 107$–111 °C, $P = 8.15$ mW
	$\theta_{ooe} = 90$ °	0.532	13 mW	0.966–1.185	cw	38 (73[a])	[93Ger]	DROPO, $T = 113$–126 °C, $L = 15$ mm, $P = 100$ mW
	$\theta = 90$ °	0.532	28 mW	1.0–1.12	cw	81	[95Bre]	DROPO, $P = 105$ mW, $L = 7.5$ mm
	$\theta_{ooe} = 90$ °	0.532	80 mW	0.788–1.640	cw	–	[98Tsu]	DROPO, $T = 80$–180 °C, $L = 15$ mm

(continued)

Table 4.1.30 continued.

Crystal	θ_{pm}, type of interaction	λ_{pump} [μm]	I_{thr} [MW cm^{-2}]	λ_{OPO} [μm]	τ_p [ns]	η [%]	Ref.	Notes
BBO	$\theta_{ooe} = 21.7$–21.9 °	0.532	278	0.94–1.22	12	10	[89Fan]	SROPO, $L = 9$ mm, $E = 1$ mJ
	ooe	0.355	130	0.45–1.68	8	9.4	[88Che]	SROPO, $L = 11.5$ mm, $E = 15$ mJ
	$\theta_{ooe} = 24$–33 °	0.355	20	0.412–2.55	2.5	24	[88Fan]	SROPO, $L = 12$ mm, $P_{av} = 140$ mW
	ooe	0.355	27	0.42–2.3	8	32	[89Bos]	SROPO, $L_1 = 11.5$ mm, $L_2 = 9.5$ mm, $\Delta\lambda = 0.03$ nm
	$\theta_{ooe} = 33.7$–44.4 °	0.355	38	0.48–0.63; 0.81–1.36	8	12	[90Bos]	SROPO, $L_1 = 17$ mm, $L_2 = 10$ mm, $\Delta\lambda = 0.05$–0.3 nm
	$\theta_{ooe} = 23$–33 °	0.355	20–40	0.402–3.036	7	40–61	[91Fix, 93Fix]	SROPO, $L = 15$ mm, $E = 0.1$–0.2
	$\theta = 28$ °	0.355	–	0.453–2.3	6	7–9	[95Joh]	SROPO, $\Delta\nu = 0.2$ cm^{-1}, $E = 100$ mJ, SHG in KDP and BBO (220–450 nm)
	$\theta = 23$–33 °	0.355	20	0.465–1.5	10	40	[94Glo]	
	$\theta = 33$ °	0.355	3.2 mJ	0.44–1.76	10	37	[97Oie]	SROPO, $L = 12$ mm, collinear and noncollinear geometries
	$\theta = 35.9$ °	0.355	–	0.5–0.7	10	–	[97Wan]	Broad spectral bandwidth OPO ($\Delta\lambda > 100$ nm) with noncollinear geometry, $L = 18$ mm
	$\theta_{ooe} = 35.5$–37 °	0.308	150	0.422–0.477	8	10	[88Kom]	SROPO, $L = 7$ mm, $E = 0.26$ mJ
	ooe	0.308	18	0.354–2.37	17	64 [a]	[91Rob]	SROPO, $L = 20$ mm, $E = 20$ mJ
	ooe	0.308	–	0.4–0.56	17	15	[93Rob]	SROPO, $L = 20$ mm, $\Delta\nu = 0.07$ cm^{-1} (with intracavity etalon)
	$\theta_{ooe} = 30$–48 °	0.266	–	0.302–2.248	7	6.3	[91Fix]	SROPO
	$\theta_{ooe} = 38.3$ °	0.266	58	0.3–2.34	4.5	15	[00Kon]	$L = 14$ mm
LBO	$\theta = 90$ °, $\varphi = 0$ °	0.78–0.81	360 mW	1.49–1.70	cw	40 [a]	[94Col1]	DROPO, $L = 2$ cm, $T = 130$–185 °C, $P = 30$ mW
	$\theta = 90$ °, $\varphi = 0$ °	0.5235	700	0.924–1.208	12	45	[93Hal2]	DROPO, $L = 12$ mm, $T = 156$–166 °C
	$\theta = 90$ °, $\varphi = 0$ °	0.5145	50 mW	0.966–1.105	cw	10	[93Col1]	TROPO, $L = 20$ mm, $T = (183 \pm 3)$ °C, $P = 90$ mW
	$\theta = 0$ °, $\varphi = 0$ °	0.5145	1 W	0.93–0.946	cw	15	[94Rob2]	SROPO, $P = 0.5$ W, $L = 25$ mm
	$\theta = 0$ °, $\varphi = 90$ °	0.364	115 mW	0.494–0.502; 1.32–1.38	cw	9.4	[93Col2, 94Col2]	SROPO and DROPO, $L = 20$ mm, $T = 18$–86 °C, $P = 103$ mW
	$\theta = 90$ °, $\varphi = 24$–42 °	0.355	14	0.435–1.922	10	22	[91Wan]	DROPO, $I_0 = 40$ MW cm^{-2}, $E = 2.7$ mJ

(continued)

Table 4.1.30 continued.

Crystal	θ_{pm}, type of interaction	λ_{pump} [μm]	I_{thr} [MW cm^{-2}]	λ_{OPO} [μm]	τ_p [ns]	η [%]	Ref.	Notes
LBO	$\theta = 0\,^\circ$, $\varphi = 0\,^\circ$	0.355	15	0.48–0.457; 1.355–1.59	12	27	[92Cui]	SROPO, T = 20–200 °C
	$\theta = 90\,^\circ$, φ = 27–42 °	0.355	60	0.455–0.655; 0.76–1.62	10	35 [a]	[93Cui]	SROPO, L = 16 mm
	$\theta = 90\,^\circ$, φ = 20.1–42.1 °	0.355	50	0.414–2.47	5	45	[94Sch]	SROPO, L = 15 mm
	$\theta = 90\,^\circ$, φ = 26–52 °	0.308	26	0.355–0.497; 0.809–2.34	17	28–40 [a]	[91Rob, 92Rob]	SROPO, L = 15 mm
	type II in XZ and YZ planes, θ = 0–9 °	0.308	30	0.381–0.387; 1.5–1.6	5	35	[91Ebr2]	L = 16 mm, I_0 = 0.1 GW cm^{-2}
	$\theta = 0\,^\circ$, $\varphi = 0\,^\circ$	0.266	10	0.314; 1.74	10	10	[92Tan]	SROPO, L = 16 mm, T = 20 °C
	$\theta = 90\,^\circ$, φ = 37–47 °	0.266	–	0.307–0.325	4	–	[94Sch]	SROPO, L = 15 mm
KTP	θ = 50–58 °, $\varphi = 0\,^\circ$	1.064	–	1.8–2.4	10	10	[90Lin1]	DROPO, E = 0.1–0.5 mJ
	$\theta = 90\,^\circ$, $\varphi = 53\,^\circ$	1.064	80	3.2	10	5	[91Kat]	SROPO, L = 15 mm, P = 0.2 W
	$\theta = 90\,^\circ$, $\varphi = 0\,^\circ$	1.06	–	1.61	15	47 (66 [a])	[93Mar1]	Diode-pumped Nd:YAG laser
	–	1.047	0.5 mJ	1.54; 3.28	18	20	[94Ter]	
	$\theta = 63.4\,^\circ$, $\varphi = 0\,^\circ$	1.047	0.6 mJ	1.58–1.84	10	40	[97Tan]	NC SROPO, L = 25 mm
	$\theta = 90\,^\circ$, $\varphi = 0\,^\circ$	0.7–0.95	70	1.04–1.38; 2.15–3.09	10	20	[92Kat]	SROPO, L = 15 mm
	$\theta = 90\,^\circ$	0.7–0.9	–	1.03–1.28; 2.18–3.03	20	55	[94Zen]	E = 49 mJ, L = 15 mm
	$\theta = 90\,^\circ$, $\varphi = 0\,^\circ$	0.769	6 mW	1.1; 2.54	cw	–	[95Sch]	TROPO, L = 12 mm
	$\theta = 54\,^\circ$, $\varphi = 0\,^\circ$	0.73–0.80	–	1.38–1.67	cw	0.001	[93Wan2]	L = 10 mm, P = 2 μW
	$\theta = 90\,^\circ$, $\varphi = 0\,^\circ$	0.532	1.4 W, SROPO; 30 mW, DROPO	1.039; 1.09	cw	35	[93Yan1, 93Yan2]	SROPO and DROPO, L = 10 mm, P = 1.07 W

(continued)

Table 4.1.30 continued.

Crystal	θ_{pm}, type of interaction	λ_{pump} [μm]	I_{thr} [MW cm^{-2}]	λ_{OPO} [μm]	τ_p [ns]	η [%]	Ref.	Notes
KTP	$\varphi = 0\,°$	0.532	80	0.7–0.9; 1.3–2.2	3.5	12	[93Bos, 92Bos]	$L = 15$ mm, $E = 3$ mJ, $\Delta\nu = 0.02$ cm^{-1}
	$\theta = 69\,°$, $\varphi = 0\,°$	0.532	–	0.75–1.04	4–6	27	[95Sri]	OPO-OPA, $L_1 = L_2 = 10$ mm, $E = 45$ mJ
	$\theta = 60\,°$, $\varphi = 0\,°$	0.532	–	0.75–0.87; 1.83–1.37	4	–	[95Hui]	$\Delta\nu = 200$ MHz (with Fabry-Perot etalon), $E = 0.6$ mJ, $L = 16$ mm
	$\theta = 90\,°$, $\varphi = 0\,°$	0.532	4.3 W	1.09; 1.039	cw	28 (64 [a])	[94Yan]	SROPO, $P = 1.9$ W, $L = 15$ mm
	$\theta = 90\,°$, $\varphi = 25.3\,°$	0.531	40 mW	1.0617	cw	30	[93Lee]	DROPO, $L = 8$ mm
	$\theta = 69\,°$, $\varphi = 0\,°$	0.532	7	0.76–1.04	6	30	[93Mar2]	$L = 15$ mm, ICSHG in BBO with $\eta = 40\,\%$ (380–520 nm)
KTA	$\theta = 53\,°$, $\varphi = 0\,°$	0.773–0.792	–	1.45; 1.7	300	0.3	[92Jan]	DROPO, $L = 7$ mm
	type II	–	–	1.11–1.20; 2.44–2.86	cw	90	[98Edw]	Intracavity (Ti:Sa) SROPO, $P = 1.46$ W, $L = 11.5$ mm
RTA	$\theta = 90\,°$, $\varphi = 0\,°$	0.77–0.83	70 mW	1.21–1.26; 2.1–2.4	cw	–	[97Sch]	SROPO, $L = 12$ mm, $P = 84$ mW, $\Delta\nu < 10$ MHz
Banana	$\theta_{ooe} = 90\,°$	0.532	–	0.75–1.82	10	5	[80Bar3]	SROPO, $T = 80$–$220\,°$C
$KNbO_3$	along the b axis	0.532	3.5	0.88–1.35	10	32	[82Kat]	DROPO, $T = 180$–$200\,°$C, $P = 12$ MW
Urea	$\theta_{oeo} = 81$–$90\,°$	0.355	55 (45 mW)	0.5–0.51; 1.17–1.22	7	20	[84Don]	SROPO, $L = 12.7$ mm, $I_0 = 90$ MW cm^{-2}
	$\theta_{oeo} = 50$–$90\,°$	0.355	–	0.5–1.23	7	23	[85Ros2, 85Ros1]	SROPO, $L = 23$ mm
	$\theta_{oeo} = 64$–$90\,°$	0.308	16–20	0.537–0.72	4–6	37	[89Ebr]	$L = 15$ mm
NPP	eeo	0.266	–	0.33–0.42	7	–	[85Ros1]	
	$\theta = 9.5$–$13\,°$, $\varphi = 0\,°$	0.5927	30	0.9–1.7	1	5	[92Jos, 93Dou]	$L = 1.9$ mm
	$\theta = 30\,°$	0.583–0.59	0.5	1–1.5	7	–	[95Kho]	

[a] Pump depletion.

Table 4.1.31. Picosecond OPO in the UV, visible, and near IR regions.

Crystal	θ_{pm}, type of interaction	λ_{pump} [μm]	I_{thr} [MW cm^{-2}]	λ_{OPO} [μm]	τ_p [ps]	η [%]	Ref.	Notes
KDP	eoe	0.532	–	0.8–1.67	40	25	[78Kry]	TWOPO, $E = 1$ mJ, $L_1 = L_2 = 4$ cm
	eoe	0.532	–	0.9–1.3	30	51	[78Dan2, 79Kab]	TWOPO, $\Delta\nu\Delta\tau = 0.7$, $L_1 = 4$ cm, $L_2 = 6$ cm, $I_0 = 15$–20 GW cm^{-2}
	eoe	0.527	–	0.82–1.3	0.3–0.5	2	[83Bar, 82Dan]	SP OPO, $E = 20$ μJ
	eoe	0.355	–	0.45–0.64, 0.79–1.69	45	15	[78Dan3]	TWOPO, $L_1 = L_2 = 4$ cm
ADP	$\theta_{ooe} = 90$ °	0.266	–	0.44–0.68	10	10	[76Mas2]	TWOPO, $T = 50$–110 °C, $L_1 = L_2 = 5$ cm
CDA	$\theta_{ooe} = 90$ °	0.532	–	0.854–1.41	10	30–60	[74Mas]	$L = 3$ cm, $T = 50$–70 °C, $I_0 = 0.3$ GW cm^{-2}
	$\theta_{ooe} = 90$ °	0.53	1000	0.8–1.3	10	12.5	[87Ion]	SP OPO, $L = 4$ cm, $I_0 = 3$ GW cm^{-2}
$LiIO_3$	ooe	0.532	–	0.61–4.25	6	4	[77Dan, 78Dan1]	TWOPO, $L_1 = 1$ cm, $L_2 = 2.5$ cm, $I_0 = 2$ GW cm^{-2}
	$\theta_{ooe} = 25$–30 °	0.53	3000	0.68–2.4	–	5	[77Kry]	TWOPO, $L_1 = L_2 = 4$ cm, $I_0 = 6$ GW cm^{-2}
$LiNbO_3$	ooe	1.06	–	1.4–4.0	3.5	10	[78Sei]	TWOPO, $\Delta\nu = 6.5$ cm^{-1}, $I_0 = 1$ GW cm^{-2}
	45–51 °	1.064	–	1.37–4.83	40	17	[77Iva]	TWOPO
	47 °	1.054	100	1.35–2.11	0.5	15	[90Lae1]	SP OPO, $L = 18$ mm, $I_0 = 0.14$ GW cm^{-2}
	84 °	0.53	–	0.66–2.7	40	17	[77Iva]	TWOPO, $T = 46$–360 °C
	90 °	0.532	–	0.68–0.76	20	9	[79Liu]	SP OPO
	90 °	0.532	8	0.85–1.4	15	17.5	[86Pis]	SROPO, $P = 30$ kW, $f = 10$ kHz
	90 °	0.532	< 30	0.65–3.0	10	7.2	[87Ion]	SP OPO, $L = 25$ mm
$LiNbO_3$:MgO	$\theta = 48.5$ °	0.75–0.84	4000	2.6–4.5	2–3	18	[96Lin]	$L_1 = L_2 = 20$ mm
	$\theta_{ooe} = 60$–84 °	0.532	–	0.7–2.2	30	5.4	[91He]	TWOPO, $\Delta\lambda = 0.3$ nm (0.7 μm) and 1.4 nm (2 μm)

(continued)

Table 4.1.31 continued.

Crystal	θ_{pm}, type of interaction	λ_{pump} [μm]	I_{thr} [MW cm^{-2}]	λ_{OPO} [μm]	τ_p [ps]	η [%]	Ref.	Notes
BBO	$\theta_{ooe} = 20.7$–22.8 °	0.532	–	0.67–2.58	18	13	[92Zhu]	TWOPO, $L_1 = L_2 = 9$ mm, $I_0 = 2.5$–3.8 GW cm^{-2}, $E = 0.1$–0.5 mJ
	ooe	0.53	–	0.63–3.2	1.3	25	[93Dan]	TWOPO-OPA, $L_1 = L_2 = 8$ mm
	ooe	0.36	500	0.406–3.17	20	30	[90Bur]	SP OPO, $L = 12$ mm, $I_0 = 2$ GW cm^{-2}, $E = 3$ mJ, $\Delta\lambda = 0.24$ nm
	$\theta_{ooe} = 26$–33 °	0.355	–	0.4–2.0	15	30	[90Hua]	OPO-OPA, $L_1 = 12$ mm, $L_2 = 6$ mm, $L_3 = 15$ mm, $I_0 = 3$ GW cm^{-2}, $\Delta\lambda = 0.3$ nm
	ooe	0.355	–	0.4–2.86	24	6.5	[90Suk]	TWOPO, $L_1 = L_2 = L_3 = 8$ mm, $I_0 = 5$ GW cm^{-2}, $\Delta\nu = 10$ cm^{-1}
	ooe	0.355	–	0.43–2.1	15	30	[93Zha1]	Injection seeding, $L = 15$ mm
	$\theta_{ooe} = 33$ °	0.3547	–	0.42–2.8	30	61	[94Hua]	OPO-OPA, $P = 51$ MW
LBO	ooe, $\theta = 90$ °, $\varphi = 0$ °	0.8	700 (400 mW)	1.15–2.26	1–2.2	27 (48 [a])	[95Ebr1]	SP OPO, $P = 325$ mW, $L = 30$ mm, $T = 120$–230 °C
	ooe, $\theta = 90$ °, $\varphi = 0$ °	0.8	320	1.374–1.53; 1.676–1.828	0.52	7.5	[95Ebr3]	SP OPO, $P = 90$ mW, $L = 16$ mm
	type I	0.77–0.8	350	1.16–2.26	1	34	[96Fre]	SP SROPO, $P = 580$ mW, $L = 16$ mm
	$\theta = 81$ °, $\varphi = 5$ °	0.57–0.63	–	1.2–1.5	0.58	10	[91Bay]	Injection seeding by 1.08 μm
	$\theta = 85$ °, $\varphi = 9$ °	0.57–0.63	–	1.2–1.5	0.4	25	[92Akh]	Injection seeding by 1.08 μm (40 ps), $L = 9$ mm, $I_0 = 1$ TW cm^{-2}
	$\theta = 90$ °, $\varphi = 0$ °	0.532	–	0.75–1.8	35	20	[91Hua]	Injection seeding OPO, $T = 106.5$–148.5 °C
	$\theta = 90$ °, ooe	0.53	–	0.65–2.5	15	24	[91Lin]	OPA, angle ($\varphi = 8.7$–15.9 °) and temperature tuning ($T = 103$–210 °C), $E = 0.45$ mJ
	$\theta = 90$ °, $\varphi = 0$ °	0.532	1500	0.77–1.7	100	30	[93Zho]	SP SROPO, $L = 15$ mm, $T = 105$–137 °C, $\Delta\lambda = 0.14$ nm
	ooe, $\theta = 90$ °, $\varphi = 11.5$ °	0.532	–	0.68–2.44	25	8	[95Liu]	$L_1 = L_2 = 15$ mm
	$\theta = 0$ °, $\varphi = 0$ °	0.532	–	0.75–1.8	15	20	[95Wal]	$P = 200$ mW, $L = 15$ mm
	$\theta = 90$ °, $\varphi = 0$ °	0.5235	2500 (10 mW)	0.652–2.65	12	13	[92Ebr2, 93Ebr, 93Hal1]	SROPO, $L = 12$ mm, $T = 125$–190 °C

(continued)

Table 4.1.31 continued.

Crystal	θ_{pm}, type of interaction	λ_{pump} [μm]	I_{thr} [MW cm^{-2}]	λ_{OPO} [μm]	τ_p [ps]	η [%]	Ref.	Notes
LBO	$\theta = 90\,°$, $\varphi = 0\,°$	0.5235	1100 (4.5 mW)	0.909–1.235	33	50	[93Hal1, 92Ebr1]	DROPO, T = 167–180 °C
	$\theta = 90\,°$, $\varphi = 0\,°$	0.5235	15 (30 mW)	0.65–2.65	1.7	50	[93Hal1]	DROPO, L = 12 mm, P = 0.21 W
	ooe, $\theta = 90\,°$, $\varphi = 0\,°$	0.5235	47 mW	0.839–1.392	1.8	70 [a]	[94Rob1]	SP SROPO, P = 88 mW, L = 3 mm
	ooe, $\theta = 90\,°$, $\varphi = 0\,°$	0.5235	170 mW	0.65–2.7	1.63	75 [a]	[95But]	SP OPO, P = 210 mW, L = 15 mm
	$\theta = 90\,°$, $\varphi = 0\,°$	0.523	100	0.72–1.91	1	34	[93McC1]	SP SROPO, L = 13 mm, T = 125–175 °C, P_{av} = 89 mW
	$\theta = 90\,°$, $\varphi = 0\,°$	0.523	80 (70 mW)	0.8–1.5	1.2–1.5	27 (75 [a])	[93But]	SROPO, L = 12 mm, P_{av} = 78 mW
	$\theta = 90\,°$, φ = 27–43 °	0.355	–	0.46–1.6	15	30	[91Zha]	Injection seeding from OPO, L = 16 mm, I_0 = 2.8 GW cm^{-2}, E = 0.3 mJ
	$\theta = 90\,°$, φ = 18–42 °	0.355	–	0.403–2.58	12	28	[92Kra]	TWOPO, $L_1 = L_2$ = 15 mm, I_0 = 5 GW cm^{-2}, E = 0.1–1 mJ
	$\theta = 0\,°$, $\varphi = 0\,°$	0.355	2300	0.4159–0.4826	30	38	[92Hua, 93Hua]	TWOPO, L = 10 mm, T = 21–450 °C, I_0 = 18 GW cm^{-2}, $\Delta\lambda$ = 0.15 nm
	$\theta = 90\,°$, φ = 30–42 °	0.355	1000	0.452–1.65	9	26	[93Agn]	DROPO, L = 10.5 mm, E = 0.15 mJ
KTP	θ = 82–90 °, $\varphi = 0\,°$	1.064	0.8 W	1.57–1.59; 3.21–3.30	2–3	15	[93Chu]	SROPO, L = 10 mm, f = 75 MHz, $\Delta\lambda$ = 1.5 nm
	–	1.064		2.128	100	25	[93Lot]	SP OPO with 6 KTP (total length 58 mm), P = 14 W
	θ = 81–90 °, $\varphi = 0\,°$	1.053	5.8 W	1.55–1.56; 3.22–3.28	12	21	[93Gra]	SP OPO, L = 6 mm, P = 2 W
	θ = 40.6–45.2 °, $\varphi = 0\,°$, oeo	0.8	–	1.02–1.16; 2.6–3.7	2.6	–	[95Gra]	OPA, E = 0.04 mJ
	$\theta = 53\,°$, $\varphi = 0\,°$, oeo	0.72–0.85	0.8 W	1.44–1.64	1.1	20	[96Qia]	SP SROPO, P = 200 mW, L = 7 mm

(continued)

Table 4.1.31 continued.

Crystal	θ_{pm}, type of interaction	λ_{pump} [μm]	I_{thr} [MW cm^{-2}]	λ_{OPO} [μm]	τ_p [ps]	η [%]	Ref.	Notes
KTP	$\theta = 90\,^\circ$, $\varphi = 0\,^\circ$	0.72–0.853	150	1.052–1.214; 2.286–2.871	1.2	42	[93Neb]	SP OPO, $L = 6$ mm, $P = 0.7$ W
	$\theta = 54\,^\circ$, $\varphi = 0\,^\circ$, eoo	0.532	250	0.614–4.16	0.39	12	[94Umb]	$L = 14$ mm
	eoe, $\theta = 90\,^\circ$, $\varphi = 35\,^\circ$	0.527	0.9 W	0.851–0.938; 1.2–1.381	2.4–3.2	13	[95Che]	SROPO, $P = 80$–280 mW, $L = 5$ mm
	$\theta = 40$–$70\,^\circ$, $\varphi = 90\,^\circ$	0.526	–	0.6–2.0	30	10	[88Van]	$L = 20$ mm
	$\theta = 40$–$80\,^\circ$, $\varphi = 0\,^\circ$	0.526	–	0.6–4.3	30	10	[88Van]	$L = 20$ mm
	$\theta = 90\,^\circ$, $\varphi = 10$–$35\,^\circ$	0.523	57 (61 mW)	1.002–1.096	2.2	16 (79 [a])	[92McC]	SP OPO, $L = 5$ mm, $P = 42$ mW
	–	0.5235	1000 (2 mW)	0.946–1.02; 1.075–1.172	8	10 (56 [a])	[91Ebr1, 93Hall]	SP SROPO, $L = 5$ mm, $P = 2$ mW
	$\theta = 90\,^\circ$	0.523	60 (61 mW)	0.938–1.184	1–2	16	[93McC2]	SROPO, $L = 5$ mm, $f = 125$ MHz, $P = 40$ mW
	$\theta = 90\,^\circ$, $\varphi = 0$–$33\,^\circ$	0.526	0.5 W	1.01–1.1	14	44	[93Gra]	SP OPO, $L = 6$ mm, $P = 0.58$ W
KTA	$\theta = 90\,^\circ$, $\varphi = 0\,^\circ$	1.064	–	1.54; 3.47	7	75	[98Ruf]	SP OPO, $L = 15$ mm
Banana	$\theta_{ooe} = 90\,^\circ$	0.532	5	0.8–1.6	10	25	[83Oni]	SP OPO
	$\theta_{ooe} = 90\,^\circ$	0.53	50	0.65–3	10	5.3	[87Ion]	SP OPO, $I_0 = 250$ MW cm^{-2}
	$\theta_{ooe} = 90\,^\circ$	0.532	7–9	0.672–2.56	15–45	8.1	[89Pis, 90Pis]	SP SROPO, $L = 10$ mm, $f = 139$ MHz, $T = 75$–$350\,^\circ$C
α–HIO_3	eoe	0.532	–	0.7–2.2	30–45	10–12	[77Dan]	TWOPO, $L_1 = L_2 = 2$ cm, $I_0 = 4$–5 GW cm^{-2}
	eoe	0.527	60	–	5–6	10	[80Bar2]	SP OPO, $\Delta\nu\,\Delta\tau = 0.7$

[a] Pump depletion.

Table 4.1.32. Femtosecond OPO in the UV, visible, and near IR regions.

Crystal	θ_{pm}, type of interaction	λ_{pump} [μm]	I_{thr} [MW cm^{-2}]	λ_{OPO} [μm]	τ_p [fs]	η [%]	Ref.	Notes
BBO	$\theta_{eoe} = 28\,^\circ$	0.78	–	1.1–2.6	60	35	[94Nis]	TWOPO, $L_1 = L_2 = 4.8$ mm, $E = 0.15$ mJ
	$\theta_{ooe} = 20\,^\circ$	0.8	–	1.2–1.3	70	5	[94Sei1]	TWOPO, $L = 4$ mm
	ooe	0.62	–	0.45–2.8	200	15	[91Joo]	TWOPO, $L_1 = 5$ mm, $L_2 = 7$ mm, $E = 20$ μJ
	ooe, eoe	0.6	–	0.75–3.1	180–250	23	[93Dan]	TWOPO-OPA, $L_1 = L_2 = 8$ mm, $I_0 = 70$ GW cm^{-2}
	$\theta_{ooe} = 19.5$–$21\,^\circ$	0.53	2200	0.68–2.4	75	30	[88Bro]	SP SROPO, $L = 7.2$ mm, $I_0 = 2.2$ GW cm^{-2}, $E = 2$ mJ
	ooe	0.527	–	0.7–1.8	65–260	3	[90Lae2, 91Lae, 93Lae]	SP SROPO, $L = 5.8$ mm
	ooe	0.527	–	1.04–1.07	70	–	[92Dub]	OPA with gain ratio 2×10^4
	$\theta_{ooe} = 32\,^\circ$	0.4	–	0.566–0.676	30	10	[94Dri]	SP OPO, $P = 100$ mW
	ooe	0.4	–	0.59–0.666	13	50	[95Gal2]	SP OPO, $P = 130$ mW
	ooe	0.395	–	0.55–0.69	14	–	[98Shi]	NC OPA, seeding with white light continuum
	$\theta_{ooe} = 32\,^\circ$	0.39	–	0.5–0.7	11	–	[97Cer]	OPA, seeding with white light continuum, $L = 1$ mm
LBO	–	0.8	–	1.1–2.4	40	38	[95Kaf]	SP OPO, $L = 6$ mm, $P = 550$ mW
	–	0.77–0.8	320	1.374–1.530; 1.676–1.828	720	7.5	[95Ebr2]	SP OPO, $P = 90$ mW
	$\theta = 90\,^\circ$, $\varphi = 0\,^\circ$	0.605	–	0.85–0.97; 1.6–2.1	200	10–15	[93Dan, 93Ban]	TWOPO, $L_1 = L_2 = L_3 = 15$ mm, $T = 30$–$85\,^\circ$C, $I_0 = 25$ GW cm^{-2}
KTP	$\theta = 43\,^\circ$, $\varphi = 0\,^\circ$, eoo	0.83	325 mW	1.05–1.16; 2.9–4.0	175	15 [a]	[95McC]	SP OPO, $L = 2$ mm
	$\theta = 90\,^\circ$, $\varphi = 0\,^\circ$, eoo	0.816	–	2.5–2.9	160	55 [a]	[95Hol]	SP OPO-OPA, $L_1 = L_2 = 0.9$ mm, $E = 0.55$ μJ
	$\varphi = 0\,^\circ$	0.765–0.815	–	1.22–1.37; 1.82–2.15	57–135	55 [a]	[92Pel]	$L = 1.15$ mm, $f = 90$ MHz, $P = 340$ mW (135 fs) and 115 mW (57 fs)

(continued)

Table 4.1.32 continued.

Crystal	θ_{pm}, type of interaction	λ_{pump} [μm]	I_{thr} [MW cm^{-2}]	λ_{OPO} [μm]	τ_p [fs]	η [%]	Ref.	Notes
KTP	$\theta = 67\,^\circ$, $\varphi = 0\,^\circ$	0.765	40000; (180 mW)	1.2–1.34; 1.78–2.1	62	–	[92Fu]	SP OPO, $L = 1.5$ mm, $f = 76$ MHz, $P = 175$ mW
	–	0.745	100 mW	0.53–0.585	200	29	[97Kar]	SP OPO with ICSHG (self-doubling OPO)
	$\theta = 45\,^\circ$, $\varphi = 0\,^\circ$	0.68	–	1.16–2.2; 0.58–0.657	57	60 [a]	[93Pow1]	$L = 1.5$ mm, $P = 0.68$ W, ICSHG in BBO ($L = 47$ μm)
	$\varphi = 0\,^\circ$	0.645	110 mW	1.2–1.34	220	13	[92Mak]	SP OPO, $P = 30$ mW
	$\theta = 53\,^\circ$, $\varphi = 0\,^\circ$	0.61	–	0.755–1.04; 1.5–3.2	105–120	–	[90Wac, 91Wac]	SP OPO in CPM dye laser cavity, $L = 1.4$ mm
	$\theta = 62\,^\circ$, $\varphi = 0\,^\circ$, eoo	0.524	2000	1.2–1.6	260	10	[95Rau]	SP OPO, $L = 3$ mm
	$\theta = 62\,^\circ$, $\varphi = 0\,^\circ$	0.5235	–	1.2–1.7	300	–	[98Lae]	SP OPO, $L = 6$ mm, $E = 10$ nJ
KTA	$\varphi = 0\,^\circ$, oeo	0.78	–	1.29–1.44; 1.83–1.91	85–150	10–15	[93Pow2]	L = 1.47 mm, P = 75 mW
RTA	$\theta = 53\,^\circ$, $\varphi = 0\,^\circ$, eoo	0.76–0.82	–	1.03–1.3; 2.15–3.65	58	25	[94Pow]	SP SROPO, $L = 1.8$ mm, $P = 250$ mW
	$\theta = 90\,^\circ$, $\varphi = 0\,^\circ$, eoo	0.78–0.86	50 mW	1.33	70	32	[95Rei]	$L = 2$ mm, $P = 185$ mW
	–	Ti:Sa	–	1.25; 2.25	78	33	[97Rei]	SP OPO, $f = 344$ MHz, $P = 0.6$ W
$KNbO_3$	$\theta = 38\,^\circ$, $\varphi = 90\,^\circ$	0.78	–	2.3–5.2	60–90	23	[95Spe, 96Spe]	$L = 1$ mm, $P = 170$–300 mW
NPP	–	0.62	–	0.8–1.6	150–290	–	[86Led, 87Led]	$L = 1.5$ mm

[a] Pump depletion.

Table 4.1.33. Optical parametric oscillation in the mid IR region.

Crystal	λ_{pump} [μm]	λ_{OPO} [μm]	τ_p	Conversion efficiency [%]	Ref.
Ag_3AsS_3	1.065	1.82–2.56	26 ns	1	[72Han]
	1.064	1.2–8	8 ps	0.01–1	[83Els]
$AgGaS_2$	1.064	1.2–10	8 ps	0.1–10	[84Els]
	1.06	1.4–4.0	18 ns	16	[84Fan]
	1.064	4.5–8.7	15–20 ps	5.4	[91Bak]
	1.064	1.16–12.9	19 ps	25	[93Kra]
	1.064	1.319; 5.505	45–80 ps	63 [a]	[94Che]
	1.047	2.6–7	0.5–2.6 ps	–	[98Lae]
	0.845	1.267; 2.535	cw	2	[98Dou]
	0.74–0.85	3.3–10	160 fs	20	[94Sei2]
$AgGaSe_2$	2.05	2.65–9.02	30 ns	> 18	[86Eck]
	2.06	~ 4.1	~ 30 ns	23	[93Bud]
	1.57	6–14	6 ns	20	[97Cha]
	1.34	1.6–1.7; 6.7–6.9	30 ns	> 18	[86Eck]
$ZnGeP_2$	2.94	5.51–5.38; 6.29–6.46	80 ps	5.3	[85Vod]
	2.94	5–5.3; 5.9–6.3	150 ps	17	[87Vod]
	2.79	5.3; 5.9	~ 100 ps	10	[93Vod2]
	2.8; 2.94	4–10	~ 100 ps	1–18	[91Vod, 93Vod1, 95Vod2]
GaSe	2.8; 2.94	3.5–18	~ 100 ps	1	[91Vod, 93Vod1, 95Vod1]
CdSe	1.833	9.8–10.4; 2.26–2.23	300 ns	40	[72Her]
	2.36	7.9–13.7	40 ns	15	[72Dav, 73Dav]
	2.87	4.3–4.5; 8.1–8.3	140 ns	15	[74Wei]
	2.87	14.1–16.4	–	–	[76Wen]

[a] Pump depletion.

4.1.8 Picosecond continuum generation

Table 4.1.34. Picosecond continuum generation in crystals.

Crystal	λ_{pump} [μm]	I_{pump} [10^9 W cm^{-2}]	λ_{cont} [μm]	η [%]	Cut angle of crystals	Ref.
KDP	1.054	50	0.3–1.1	10	$\theta = 49°$	[83Mur]
KDP	0.527	30–40	0.84–1.4	15	$\theta = 42°$	[82Bar]
$LiIO_3$	0.355	–	0.46–1.55	–	$\theta = 90°$	[85Pok]
$LiIO_3$	0.532	0.3	0.67–2.58	–	$\theta = 90°$	[85Pok]
$LiIO_3$	1.064	–	1.72–3.0	–	$\theta = 90°$	[85Pok]
$LiNbO_3$	1.064	–	1.92–2.38	3	$\theta = 44.7°$	[75Cam]
GaAs	9.3	100	3–14	–	–	[85Cor]